



On-board reagent storage and release by solvent-selective, rotationally opened membranes: a digital twin approach

Jens Ducreé¹

Received: 8 October 2021 / Accepted: 21 December 2021 / Published online: 26 April 2022
© The Author(s) 2022

Abstract

Decentralized bioanalytical testing in resource-poor settings ranks among the most common applications of microfluidic systems. The high operational autonomy in such point-of-care/point-of-use scenarios requires long-term onboard storage of liquid reagents, which also need to be safely contained during transport and handling, and then reliably released just prior to their introduction to an assay protocol. Over the recent decades, centrifugal microfluidic technologies have demonstrated the capability of integrated, automated and parallelized sample preparation and detection of bioanalytical protocols. This paper presents a novel technique for onboard storage of liquid reagents which can be issued by a rotational stimulus of the system-innate spindle motor, while still aligning with the conceptual simplicity of such “Lab-on-a-Disc” (LoaD) systems. In this work, this highly configurable reagent storage technology is captured by a digital twin, which permits complex performance analysis and algorithmic design optimization according to objectives as expressed by target metrics.

Keywords Reagent storage · Centrifugal microfluidics · Lab-on-a-Disc · Rotational actuation · Process integration · Digital twin

1 Introduction

The automation of bioanalytical assay panels has been a paramount objective of microfluidic technologies since their debut in the early 1990s (Manz et al. 1990; Auroux et al. 2002; Reyes et al. 2002; Whitesides 2006; Janasek et al. 2006). In the meantime, these Lab-on-a-Chip devices have pervaded manifold application spaces, primarily in biomedical point-of-care and global diagnostics, liquid handling automation for the life sciences, process analytical techniques and cell line development for biopharma, as well as monitoring the environment, infrastructure, industrial processes and agrifood (Gijs et al. 2010; Nge et al. 2013; Liu et al. 2014; Mauk et al. 2017; Yuan and Oleschuk 2018; Olanrewaju et al. 2018). Compliance with the relevant workflows, infrastructure, operator skill and competitive cost of ownership/per test are vital for their deployment in locations outside sophisticated medical infrastructure.

Various miniaturized liquid handling platforms have been introduced, which may be distinguished by their pumping

scheme; among them are pressure sources, capillary force, electrokinetics, electrowetting on dielectric, bulk and surface-acoustic waves. Throughout the last about 30 years, centrifugal microfluidic platforms have been at the center of commercial and academic endeavors. Driven by a rugged spindle motor, these low-complexity “Lab-on-a-Disc” (LoaD) systems (Schembri et al. 1992, 1995; Abaxis (Piccolo Express) 2021; Andersson et al. 2007; Inganas et al. 2005; Gyros Protein Technologies 2021; Madou and Kellogg 1998; Shea 2003; Smith et al. 2016a; Kong et al. 2016a; Maguire et al. 2018; Gorkin et al. 2010a; Burger et al. 2016; Aeinehvand et al. 2018; Sciuto et al. 2020; Ducreé 2021a; Ramachandraiah et al. 2013; Thompson et al. 2016a; Krauss et al. 2019; Abi-Samra et al. 2011a; Thompson et al. 2016b; Watts et al. 2007; Kim et al. 2013; Moschou et al. 2006) excel through their high-performance centrifugal sample preparation, and their modular setup featuring an instrument (“player”) spinning a microfluidic disc carrying the sample and reagents.

Mostly operating in batch-mode, biosamples are pre-conditioned through a series of centrifugally implemented Laboratory Unit Operations (LUOs), such as metering (Mark et al. 2008; Keller et al. 2015), mixing (Grumann et al. 2005; Ducreé et al. 2006a, b; Burger et al. 2020), incubation, purification/concentration/extraction (Strohmeier et al. 2015a;

✉ Jens Ducreé
jens.ducree@dcu.ie

¹ School of Physical Sciences, Dublin City University, Glasnevin, Dublin 9, Ireland

Brassard et al. 2019), homogenization (Karle et al. 2009; Kido et al. 2007), particle filtering (Haeberle et al. 2006; Steigert et al. 2007; Kinahan et al. 2016a; Dimov et al. 2014; Gaughran et al. 2016; Zehnle et al. 2017), and droplet generation (Haeberle et al. 2007; Schuler et al. 2015, 2016), while transiently held back in each step by a downstream valve. Note that some assay steps may also be realized by transferring functionalized magnetic particles between reagent chambers (Czilwik et al. 2015; Grumann et al. 2004).

Akin to the pick-up heads familiar with digital data storage technologies like CD, DVD or Blu-ray, most read-out schemes for LoaD systems are based on optical detection (Maguire et al. 2018; Gorkin et al. 2010a; Burger et al. 2016; Ducrée et al. 2007; Lutz et al. 2011; Tang et al. 2016; Duffy et al. 1999; Azimi-Boulali et al. 2020; Strohmeier et al. 2015b; Kong et al. 2016b; Aeinhevand et al. 2017, 2019; Hess et al. 2019; Nguyen et al. 2019; Rombach et al. 2020; Homann et al. 2021; Madadelahi et al. 2020; Miyazaki et al. 2020; Brennan et al. 2017; Delgado et al. 2016). While the radially directed, outwards pointing centrifugal field is independent of the outer contours of the microfluidic chip, a disc shape complies with the rotational symmetry and supports mechanical balance, layout, and mold flow in common mass manufacturing schemes such as (compression-)injection molding; yet, deviations from the common 12-cm diameter and 1.2-mm thick CD format are quite common, e.g., smaller “mini-discs”, disc segments, tubes (Kloke et al. 2014; Mark et al. 2009a; Haeberle et al. 2008), or rectangular, e.g., microscope slides (Morais et al. 2006). Furthermore, the alignment of the inlet ports, outlets and detection chambers may also be important for seamless interfacing with standard well-plate formats, liquid handling robotics, and associated equipment like readers. For simplicity, we refer to all these LoaD variants as “discs” in the following.

Liquid volumes concurrently residing on a rotor experience the same spin rate, and are thus simultaneously driven by the rotationally induced centrifugal field, which further depends on their individual radial locations. Hence, and other than for most conventional Lab-on-a-Chip systems, valving represents a key ingredient for automating sequential liquid handling protocols of the LoaD. In principle, the disc could be halted for valve opening, for instance, by a manual or instrument-based, e.g., mechanical, thermal or radiation-based actuator (Mishra et al. 2017; Kinahan et al. 2016b; SpinX Technologies 2021; Abi-Samra et al. 2011b; Kong et al. 2015; Al-Faqheri et al. 2013; García-Cordero et al. 2009, 2010; Torres Delgado et al. 2018). However, it is often preferable to keep the disc-based liquid volumes at bay through, at least moderate, centrifugation; such suppression of flow during spinning involves co-rotating power sources, e.g., pneumatic pumps (Clime et al. 2015, 2019) or electro-thermal or radiative units for melting sacrificial barriers film (Torres Delgado et al. 2018; Kinahan et al. 2018; Delgado et al. 2018).

However, this work focuses on rotationally controlled valving concepts, which have been chosen by many researchers by virtue of to their smooth alignment with the low overall complexity of the LoaD platform (Ducrée 2021b). In these passive valves, the centrifugal pressure head propelling liquid segments towards the perimeter of the disc is combined with other pressure contributions that are independent of external power. In their high-pass variants, the centrifugal driving force is, for instance, opposed by a capillary barrier, while low-pass siphon valves typically feature hydrophilic coatings in their inbound sections, or pneumatic effects, so that valving is ushered in by reducing the spin rate below a critical threshold. In addition, various centrifugo- or thermo-pneumatic flow control mechanisms (Godino et al. 2013; Schwemmer et al. 2015a, 2015b; Zhao et al. 2015; Zehnle et al. 2015; Henderson et al. 2021; Gorkin et al. 2012; Kinahan et al. 2014, 2015; Mishra et al. 2015) have been engineered for creating forward or reverse pressure differentials.

To provide full-fledged sample-to-answer automation for conforming with the needs of point-of-care applications, the disc has to be pre-loaded with liquid or dry reagents; this way the user only needs to introduce the sample while being relieved from dealing with the logistics and loading of reagents from separate stocks. In addition to the capabilities of many techniques conceived for temporarily retaining liquid volumes while carrying out LUOs along with assay protocols, valves for longer-term storage also need to impede evaporation, diffusion into the bulk material, or exposure to ambient contaminants and humidity over shelf lives of many months, sometimes even years, and possibly even harsh ambient conditions and rough handling during transport.

In addition to (dry) storage within matrices (Zhang et al. 2016; Hin et al. 2018; Eker et al. 2014; Rombach et al. 2014; Tijero et al. 2015), liquid buffers and reagents have been retained by physical barriers (Deng and Jiang 2019), like flexible membranes (Baier et al. 2009; Margell et al. 2008; Czurratis et al. 2015; Kazemzadeh et al. 2019), blisters/pouches (Smith et al. 2016b), ampoules (Krauss et al. 2019; Hoffmann et al. 2010), cartridges (Kloke et al. 2014; Li et al. 2020), or wax plugs (Abi-Samra et al. 2011b; Kong et al. 2015; Al-Faqheri et al. 2013; Wang et al. 2019); similar to the previously discussed active valves, these containers may be opened by stimuli such as mechanical piercing, illumination by a high-power laser, or by local heating. Further performance criteria of suitable reagent storage valves are their compatibility with manufacture and assembly, the suppression of possible leaching of chemicals from solids during extended periods of phase contact. Last but not least, the fluidic performance needs to be assured in terms of the reliability of the release mechanism, and the recovery ratio, accuracy, and precision of the delivered liquid volume.

Dovetailing the centrifugal microfluidics covered in this work, also directly rotationally induced opening is, at least theoretically, possible. Yet, for existing mechanisms,

it needs to be considered that, e.g., for limited motor power and safety, there is an upper limit for practically achievable spin rates, and the reservoir might have to be placed centrally, which would severely restrict obtainable pressure heads to fractions of common atmospheric pressures. Thus, the valve controlling the reagent reservoir has to yield at rather small pressure heads. Reliability is additionally impaired as the mechanical strength of a required designated mechanical weak or yield point is hard to define, thus smearing out the associated spin frequency threshold for triggering liquid release. Critical operational robustness hence demands setting a high rotational speed for opening, which tends to counteract the options for fluidic multiplexing of concurrently loaded liquids (Ducrée 2021a, c).

This paper focuses on a novel type of rotationally actuated valve; during storage of an aqueous reagent, a (water) dissolvable film (DF) presents a diffusion barrier which is initially protected by an oleophilic, ancillary liquid having a certain, specific density (Gaughran et al. 2016; Mishra et al. 2015, 2017, 2020; Ducrée 2021d; Lu et al. 2020). Upon spinning, a centrifugo-hydrostatic equilibrium is reached, in which the interface between the two immiscible liquids contacts and thus dissolves the DF. In an idealized model, the reagent will be issued at any finite spin rate situated within its practical limits imposed by motor power, operational robustness and safety.

In addition to the general prerequisites for on-board storage of liquid (and potentially also for protecting dry / lyophilized) reagents, such valves need to meet further specifications. During logistics and manual handling, acceleration due to shaking and terrestrial gravity act on the liquid volumes, while the meniscus between the immiscible fluids needs to stay near its default rest position to prevent premature opening. Moreover, manufacturing and dispensing precision, evaporation rates, and structural fidelity affect the release mechanism, and potentially enclosed or emerging gas bubbles need to be tolerated.

This work first elaborates the operational principles for rotationally controlled on-board storage and release valving enabled by an immiscible ancillary liquid. In the initial section, strategic features of the basic layout are introduced, and first motivated in a mostly qualitative manner. Next, design objectives are quantified in terms of key performance indicators. The individual or collective optimization of these “KPIs” is implemented based on a “digital twin” (Digital Twin 2021; Marr 2017; Grieves et al. 2017), which constitutes a virtual representation of a real-world physical system derived on the underlying functional model. The digital twin method allows virtualizing the optimization of the novel reagent storage technology, thus substantially reducing cost and time scales for product development.

2 Working principle

Figure 1 illustrates the fundamental mechanism underpinning storage and release of liquid reagents described in this work. In the portrayed, exemplary fluidic structure, which is referred in the following to as Γ , two reservoirs of upper and lower cross sections A and a , and heights H and h on the left, and A' and a' , and H' and h' on the right, hold the aqueous reagent and the immiscible ancillary liquid of densities ρ and ρ' , respectively. These containers are interconnected by an isoradial channel placed at an (inner) radial position R of axial length \mathcal{L} , radial height \mathcal{H} , and of cross section \mathcal{A} , which accommodates a water-dissolvable film (DF) of axial extension δz at the (mean) position \mathcal{Z} on the z -axis.

For the duration of storage and transport ($\omega = 0$), the phase interface between the immiscible liquids must reside within a (coaxial) segment of a cross section \mathcal{a} of axial length δz , at a target position $z = \mathcal{Z}$, or at least $|z - \mathcal{Z}| \leq 0.5 \cdot \delta z$. For activation and release in hydrostatic equilibrium at an angular spin rate $\omega = 2\pi \cdot \nu > 0$, the meniscus needs to move beyond the location of the DF at $z = \mathcal{Z}$.

The conservation of liquid volumes is generally expressed as

$$U(\check{r}, \hat{r}) = \int_{\check{r}}^{\hat{r}} A(r) dr \tag{1}$$

for general geometries Γ by the integral over the function $A(r)$ representing the dependence of the (compartmentalized) cross section A on the radial coordinate r between the inner and outer radial confinements of the liquid distributions Λ or Λ' ; this liquid volume U (1) spans between its inner and other radial confinements \check{r} and \hat{r} , respectively.

To simplify the math without compromising the outcomes of this work, we consider a structure Γ composed of cuboidal segments in Fig. 1, with $\check{r} = r_0$ or r (and r'_0 and r' for the ancillary liquid), and $\hat{r} = R + \mathcal{R}$ (for both arms). Instead of having to (numerically) solve the possibly complex integral $U(\check{r}, \hat{r})$ in (1), the liquid volumes can then be expressed (assuming $R - h - H \leq r \leq R - h$) by the algebraic formulas

$$U = A \cdot (R - h - r) + a \cdot h + \mathcal{A} \cdot z \Rightarrow r = r(U, R, \Gamma, z) \tag{2}$$

for the aqueous reagent and (assuming $R - h' - H' \leq r' \leq R - h'$)

$$U' = A' \cdot (R - h' - r') + a' \cdot h' + \mathcal{A} \cdot (L - z) \Rightarrow r' = r'(U', R, \Gamma, z) \tag{3}$$

for the ancillary liquid. Equations (2) and (3) link the loaded liquid volumes U and U' to the radial position R of Γ , their structural parameters $A, A', a, a', h, h', \mathcal{A}, \mathcal{a}, z, \delta z$ and \mathcal{L} as represented by Γ , their liquid levels r and r' , and their phase interface at $0 < z < \mathcal{L}$; the liquid levels at rest can therefore be expressed as $r = r(U, R, \Gamma)$ in (2) and $r' = r'(U', R, \Gamma)$ in (3).

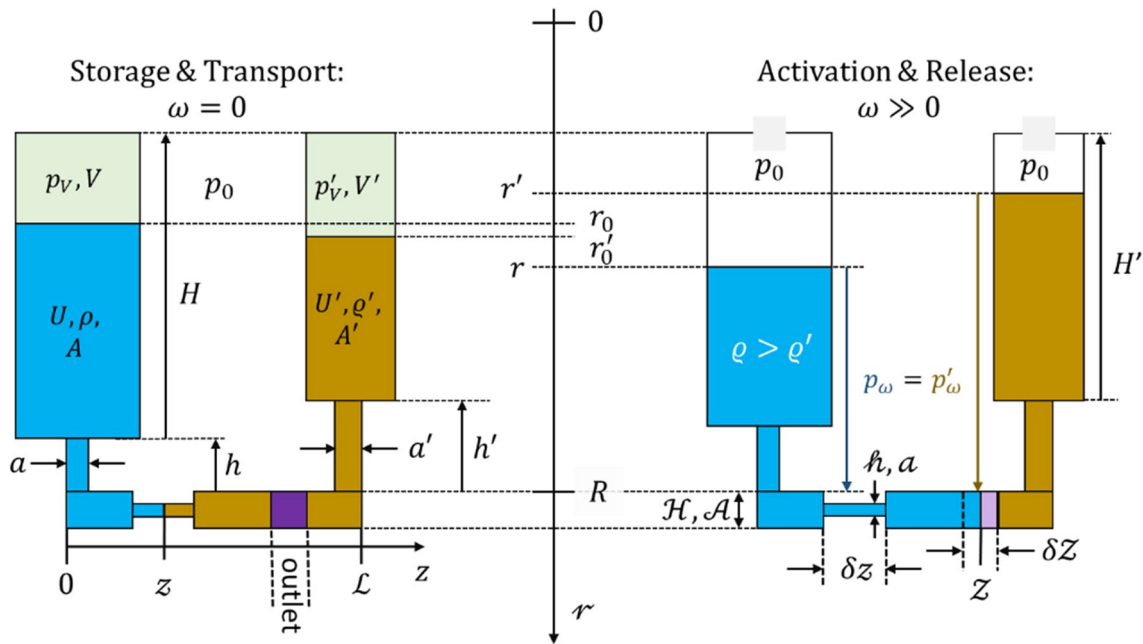


Fig. 1 Basic storage and release mechanism (linearized, 2-dimensional display of cylindrical coordinates, dimensions not to scale). The two-pronged structure, referred to as Γ , is divided into upper and lower radial sections of cross sections A and A' , and a and a' , and heights of H, H', h and h' , respectively. An isoradial channel at an inner radial position R possesses an axial length L , a radial extension \mathcal{H} and cross section \mathcal{A} ; a section of radial height h , cross section ω and length $\delta z < L$ is centered at z to provide a further degree of freedom. (Left) In a first step at rest ($\omega = 0$), the aqueous reagent and an immiscible ancillary liquid of volumes U and U' , densities ρ and ρ' , and viscosities η and η' , are loaded to the left and right reservoirs with initial meniscus positions r_0 and r'_0 of their liquid distributions $\Lambda(\omega)$ and $\Lambda'(\omega)$, respectively; their phase interface z is targeted to be located within the center of the z -segment of axial length δz and centered at $z = z$ in the isoradial channel, or at least $|\tilde{z} - z| \leq 0.5 \cdot \delta z$. These compartments are then isolated at pneumatic pressures $p_{V(\omega=0)} = p'_{V(\omega=0)} = p_0$ (9) from the ambient pressure at $p_0 \approx p_{std} = 1013.25$ hPa. (Right) Before

its (default) on-site usage, both seals are removed from the disc. During rotation at (theoretically any) $\omega > 0$, the initial difference $\Delta p_{\omega}(\rho, \rho', U, U', R, \Gamma, \omega, z) = p_{\omega}(\rho, U, R, \Gamma, \omega, z) - p_{\omega}(\rho', U', R, \Gamma, \omega, z) > 0$ resulting from the pressure heads p_{ω} (4) drives the liquid distributions $\Lambda(\omega)$ and $\Lambda'(\omega)$ towards hydrostatic equilibrium $\Delta p_{\omega}(\rho, \rho', U, U', R, \Gamma, \omega, z) = 0$ (4), and consequently to new inner meniscus positions $r > r_0$ and $r' < r'_0$. For triggering the reagent release through an outlet, e.g., located in a lower disc layer connected by a vertical via, the liquid–liquid interface at $z = z(\rho, \rho', U, U', R, \Gamma, \omega)$ in hydrostatic equilibrium needs to cover the DF at $z = z$, which features an axial extension δz , that was so far protected by the ancillary liquid, i.e., $z \geq z$. Note that the geometry Γ is deliberately composed of cuboid segments to facilitate calculations. The default values for the parameters indicated are compiled in Table 1. Evidently, by suitably adjusting the dissolution characteristics of the DF, also non-aqueous liquids may be stored and released with the same mechanism

2.1 Loading, storage and transport

Following a suitable, well-reproducible, possibly closed-loop controlled experimental loading procedure at $\omega = 0$, the two liquids are introduced at ambient pressure p_0 (typically $p_0 \approx p_{std}$ with the standard atmospheric pressure $p_{std} = 1013.25$ hPa) to place the phase interface at z within the center of the isoradial segment at z . For a starting position $z = z$ of the initial interface after properly loading U and U' at $\omega = 0$, the conservation of mass (1) trivially yields the initial filling levels $r_0 = r_0(U, \Gamma, Z)$ and $r'_0 = r'_0(U', \Gamma, Z)$. To suppress evaporation and contamination during subsequent storage, transport and handling, each reservoir is then isolated from ambient by a membrane exhibiting good barrier properties.

2.2 Liquid release

In response to spinning at a finite spin speed $\omega > 0$, the centrifugal pressure heads

$$p_{\omega} = \rho \cdot \bar{r} \Delta r \cdot \omega^2 \text{ and } p'_{\omega} = \rho' \cdot \bar{r}' \Delta r' \cdot \omega^2 \tag{4}$$

are induced to move and reshape the liquid distributions Λ and Λ' , which are then confined by their (inner) menisci at the radially inner r, r' and common outer positions R , respectively. (Note that $\mathcal{H}/R \ll 1$ and $h/R \ll 1$ are assumed throughout.) The products $\bar{r} \Delta r$ and $\bar{r}' \Delta r'$ in (4) are composed of the mean radial positions $\bar{r} = 0.5 \cdot (R + r)$ and $\bar{r}' = 0.5 \cdot (R + r')$, and the liquid level differences $\Delta r = R - r$ and $\Delta r' = R - r'$.

In default actuation mode, the pneumatic seals are removed from the disc prior to launching the centrifugal assay protocol $\omega(t)$. While rotating at sufficiently high ω , so that $p_\omega \propto \omega^2$ (4) overcomes unfavorable stiction and capillary effects occurring in real-world systems, a hydrostatic equilibrium

$$\Delta p_\omega = p_\omega - p'_\omega \tag{5}$$

establishes which can be rewritten

$$\rho \cdot (R + r) \cdot (R - r) = \rho' \cdot (R + r') \cdot (R - r') \tag{6}$$

and therefore only relates the two liquid levels $r = r(\rho, \rho', U, U', R, \Gamma)$ and $r' = r'(\rho, \rho', U, U', R, \Gamma)$ to the radial position R of Γ , the loaded liquid volumes U and U' , and their densities ρ and ρ' , but not to ω . The new, centrifugally stabilized position of the phase interface is defined by $\Delta p_\omega(\rho, \rho', U, U', R, \Gamma, z) = 0$ (5), and hence directly obtained from r and Γ , i.e., $z = z(\rho, \rho', U, U', R, \Gamma)$.

Consequently, the centrifugally triggered release through the DF at \mathcal{Z} comes down to $z \geq \mathcal{Z}$, which predicates on $\Delta p_\omega(z) > 0$ (5) during the transition of the meniscus at z all along the way from the position during storage at \mathcal{z} to the DF at $\mathcal{Z} > \mathcal{z}$. This condition implies that a minimum reagent volume

$$U_\Delta(z) = \int_{\mathcal{z}}^z A(\mathfrak{z}) d\mathfrak{z} = 0.5 \cdot a \cdot \delta z + \mathcal{A} \cdot (z - \mathcal{z} - 0.5 \cdot \delta z) \tag{7}$$

(for $z + 0.5 \cdot \delta z \leq z \leq \mathcal{Z}$) needs to be displaced for valve opening, and the shift of the left liquid level from r_0 to $r > r_0$, while the meniscus of the ancillary liquid moves radially inbound from r'_0 to $r' < r'_0$. Given that all meniscus positions r_0, r, r'_0 and r' remain in their respective inner compartments of cross sections A and A' during this reconfiguration of the liquid segments towards centrifugo-hydrostatic equilibrium from $z = \mathcal{z}$ to \mathcal{Z} , we obtain $r = r_0 + U_\Delta(\mathcal{Z})/A$ and $r' = r'_0 - U_\Delta(\mathcal{Z})/A'$.

2.3 Reliability

In practical applications, tolerances, mainly in the geometrical dimensions, as quantified by the standard deviations here collectively referred to as $\Delta\Gamma$, and in the liquid volumes ΔU and $\Delta U'$ after pipetting, impact the spread Δz of the interface z from their target positions \mathcal{z} and \mathcal{Z} at $\omega = 0$ and $\omega > 0$, respectively. Using (5), (2) and (3) for the meniscus position $z = z(\rho, \rho', U, U', R, \Gamma)$, its standard deviation

$$\Delta z \left(\left\{ \frac{\partial z}{\partial \gamma_k} \right\}, \{ \Delta \gamma_k \} \right) = \sqrt{\left(\sum_k \frac{\partial z(\rho, \rho', U, U', R, \Gamma)}{\partial \gamma_k} \cdot \Delta \gamma_k \right)^2} \tag{8}$$

depends on the partial derivatives $\partial z / \partial \gamma_k$ with $\gamma_k \in \{\rho, \rho', U, U', R, \Gamma\}$, and the standard deviations $\Delta \gamma_k \in \{\Delta \rho, \Delta \rho', \Delta U, \Delta U', \Delta R, \Delta \Gamma\}$, evaluated at the critical positions \mathcal{z} and \mathcal{Z} , respectively. Note that strictly speaking, Eq. (8) only holds for small deviations $\{\Delta \gamma_k\}$. Alternatively, as used for robustness analysis further below, Monte-Carlo methods (see Fig. 7 below) can be employed to compute Δz at the two target positions $z = \mathcal{z}$ and \mathcal{Z} .

According to this functional model, operational robustness during storage, transport and rotation caused by statistical variations $\{\Delta \gamma_k\}$ is tightly linked to squeezing the interval of the actual interface positions $z \pm 0.5 \cdot M \cdot \Delta z$ (8) within the narrow segment after loading at rest, i.e., $M \cdot \Delta z(\omega = 0) < 0.5 \cdot \delta z$, and for reliable release at $\omega > 0$, $M \cdot \Delta z(\omega > 0) < 0.5 \cdot \delta \mathcal{Z}$. The factor M quantifies the targeted degree of operational robustness, with 68%, 95%, 99.7%, 99.99%, ... for $M \in \{1, 2, 3, 4, \dots\}$.

3 Design characterization and optimization

The digital twin (Ducrée 2021b; Digital Twin 2021; Marr 2017) developed here allows to configure the free experimental parameters $\{\gamma_k\}$ for achieving key performance goals,

while staying commensurate with design-for-manufacture and scale-up of fabrication (Ducrée 2019). Such design optimization is facilitated by the multi-segmented structure Γ (Fig. 1) featuring cross sections $A, a, A', a', \mathcal{A}$ and \mathcal{a} with respect to the axial direction (and their respective axial heights / lengths $H, h, H', h', \delta z$ and \mathcal{L}). The core motivation of this draft layout is now briefly outlined on a qualitative, heuristic manner; note that due to the huge variety of possible application cases in the multi-dimensional parameter space $\{\rho, \rho', U, U', R, \Gamma\}$, only computational optimization towards well-defined target metrics is likely to lead to good-quality results.

The liquid volumes U and U' are chosen to settle the menisci r and r' in the inner (wider) region of their reservoirs with cross sections A and A' , so that effects of volume deviations, whether related to systematic loss by evaporation or dispenser precision ΔU and $\Delta U'$, on the initial liquid levels r_0 , and r'_0 , and thus the centrifugal equilibrium (5) determining z at $\omega > 0$, are largely mitigated. For given volumes U and U' , the lower radial segments of the reservoirs display smaller cross sections a and a' ; for instance, $a < A$ amplifies $\Delta r = r' - r$, and thus the net pressure $p_\omega \propto \Delta r$ (4) for pumping the minimum volume fraction U_Δ (7) of U to reach $z = \mathcal{Z}$, as required for prompting disintegration of the DF.

The additional segment centered at z in the isoradial channel featuring a cross section a over an axial extension δz has been introduced for supporting the definition of the liquid–liquid interface, and to suppress the shift of the meniscus by a high flow resistance scaling with $\delta z/a^2$ during storage and transport. Evidently, it is critical that the actual position of the meniscus at \tilde{z} , when factoring in experimental tolerances in $\{\rho, \rho', U, U', R, \Gamma, \}$, remains between the edges, i.e., $|\tilde{z} - z| < 0.5 \cdot \delta z$ (while avoiding enclosure of gas between the liquid phases). A large extension δz is desirable for improving the tolerance to discrepancies in the loading procedure of the two liquids.

3.1 Loading

The reservoirs are filled at the factory (while $\omega = 0$) with the two immiscible liquids, in the main exemplary case considered here with water and FC-72 (3 M™ Fluorinert™ Electronic Liquid FC-72), of target volumes U and U' and densities ρ and ρ' through their designated inlet ports. The loading procedure should be highly reproducible, and ideally be monitored until the actual meniscus location \tilde{z} matches z , or at least settles sufficiently central in their designated channel section around z , i.e., $|\tilde{z} - z| \ll 0.5 \cdot \delta z$. For the low contact angles that are often observed between an oil-based ancillary liquid and the polymer surface, it is advisable to first load the aqueous phase or to coat the wall with a suitable agent.

3.2 Transport

When taken out of its storage, a Load may experience various accelerations β , e.g., repetitively during manual handling, walking or in a moving vehicle, or punctually and more forcefully when its full weight hits solid ground, e.g., after falling from a height. The directions of the resulting, usually unintended forces tend to be oriented randomly but may possess components parallel to the designated radial axis during spinning. The unknown number, magnitude, orientation and duration of such arbitrary inertial effects make it impossible to exactly quantify their impact on the deviation of the actual meniscus position \tilde{z} from its target value. As successive accelerations might point in opposite directions, and thus somewhat neutralize their effect on the meniscus position, it is mostly likely that a single hard impact aligned in r -direction will compromise the liquid distributions Λ and Λ' . We consider here two main mechanisms for pinning the phase interface during transport.

3.2.1 Pneumatic stabilization

Air-tight membranes seal the inlet ports of the reservoirs after loading the reagent and ancillary liquid to prevent

evaporation. In addition, these fluid barriers also pneumatically stabilize Λ and Λ' by virtue of Boyle's law

$$p_V = p_0 \cdot \frac{V_0}{V} \tag{9}$$

stating that a change of an originally confined gas volume V_0 at p_0 to V alters the pressure to $p_V \neq p_0$ (9). So, for instance, according to the conservation of liquid volume $dU/dt = 0$ (1), transport-related disruption may induce a shift of the liquid level r on the (left) aqueous side towards the center of rotation, which ensues a peripheral displacement of the liquid level r' of the ancillary fluid (right) towards R (Fig. 1).

The resultant changes in the gas volumes V and V' lead to an increase in p_V and a reduction of $p_{V'}$, thus seeking to restore $\tilde{z} \mapsto z$. The driving pressure (difference)

$$\begin{aligned} \Delta p_V(z) &= p'_{V'}(z) - p_V(z) = p_0 \cdot \left[\frac{V'_0}{V'(z)} - \frac{V_0}{V(z)} \right] \\ &= p_0 \cdot \left[\frac{V'_0}{V'_0 - U_{\Delta}(z)} - \frac{V_0}{V_0 + U_{\Delta}(z)} \right] \end{aligned} \tag{10}$$

should consequently be maximized through adjusting the z -dependent, displaced liquid volume $U_{\Delta}(z)$ in (7), and the initial gas volumes V_0 and V'_0 underneath the seal for steadying the interface position near $z = z$ during transport. Figure 2(left) illustrates the dependency of the effective counter pressure Δp_V (10) in response to (left) a shift z from the default $z = 10$ mm. Figure 2(right) reveals that the restoring pressure $\Delta p_V < 0$ (10), evaluated at the downstream boundary of the z -segment $z = z + 0.5 \cdot \delta z$, approaches 0 towards scaling the initially enclosed gas volumes V_0 and V'_0 by the (same) factor ξ .

3.2.2 Geometrical factors

It would be disastrous from an operational point of view if the full volume $U_{\Delta}(z)$ in (7) was displaced so that the aqueous reagent already reaches $z \geq Z$ to open the DF during storage, transport and handling. This fatal event would happen in case the liquid distributions Λ and Λ' experienced an acceleration β with a strong component parallel to the radial r -direction of the centrifugal field (Fig. 1) for a sufficiently long duty cycle τ . Note that even though not discussed here for the sake of clarity, the interface may also leave the designated isoradial region, i.e., $z > z + 0.5 \cdot \delta z$, under the impact of β to disrupt the phase interface.

In response to an acceleration β with a major component parallel to the radial r -axis, the liquid distributions Λ and Λ' seek hydrostatic equilibrium (5). The resulting flow is driven by the pressure differential

$$p_{\beta} \approx \beta \cdot [\rho \cdot \Delta r - \rho' \cdot \Delta r'] \tag{11}$$

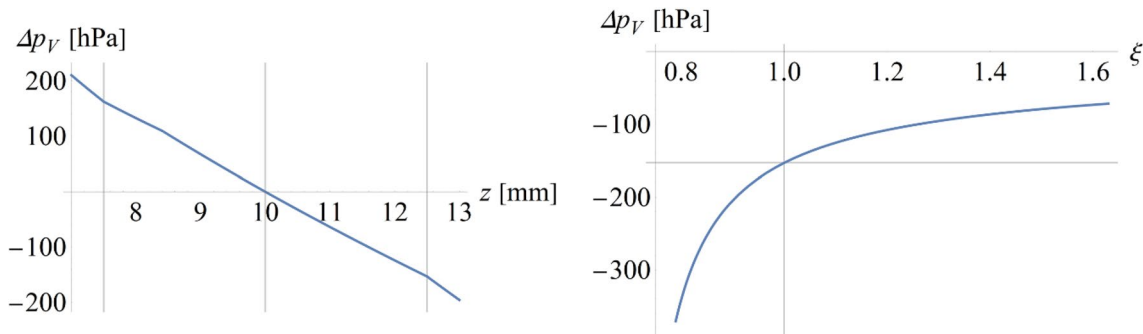


Fig. 2 Net pneumatic (counter-)pressure Δp_V (10) as a function of (left) the axial coordinate z with the equilibrium $\Delta p_V = 0$ at $z = z$, and (right) scaling the initial volumes V_0 and V'_0 by applying a factor ξ to their heights while pinning the meniscus position at the end of

the z -section $z = z + 0.5 \cdot \delta z$. Reducing the initial gas volumes V_0 and V'_0 hence stabilizes the actual meniscus position \tilde{z} in the vicinity of z during transport. Default values (Table 1) are used in this example

(initially) applying along the axial z -axis towards Z , and throttled by the aggregate hydrodynamic resistance

$$\mathcal{R} = \sum_q \mathcal{R}_q = \sum_q c_q \cdot \frac{\eta_q \cdot l_q}{A_q^2} \tag{12}$$

of the structural segments indexed by q , possessing a cross section A_q , and filled over an axial length l_q with the reagent and ancillary liquid with viscosities η or η' , respectively. The numerical coefficients c_q amount to 8π for round cross sections. This law of Hagen-Poiseuille delivers a volume flow rate

$$\dot{U}_V = \frac{dU}{dt} = \frac{p_\beta}{\mathcal{R}} \approx \frac{\beta \cdot [\varrho \cdot \Delta r - \varrho' \cdot \Delta r']}{\sum_q c_q \cdot \eta_q \cdot l_q / A_q^2} \tag{13}$$

which is governed by p_β (11) and $\{\mathcal{R}_q\}$ (12). As the outlet opens for $\dot{U}_V \cdot \tau \geq U_\Delta(z)$ in (7), the duty cycle $\tau = U_\Delta / \dot{U}_V$ ought to be maximized to best suppress operationally disastrous premature release of reagent during transport. However, since β is unknown, we define a resilience (evaluated for $z = Z$)

$$\tau_\beta = \frac{\tau}{\beta} = \frac{U_\Delta}{\beta \cdot \dot{U}_V} \approx \frac{\sum_q c_q \cdot \eta_q \cdot l_q / A_q^2}{[\varrho \cdot \Delta r - \varrho' \cdot \Delta r']} \cdot [0.5 \cdot a \cdot \delta z + \mathcal{A} \cdot (Z - z - 0.5 \cdot \delta z)]$$

expressed in units of $s^3 \cdot m^{-1}$, to be maximized by adjusting to the structure Γ (Fig. 1) for mitigating unfavorable effects owing to transport conditions.

This design goal of maximizing τ_β (14) translates into enlarging the dead volumes $U_\Delta(Z)$ (7) of the isoradial channel extending between $Z = z$ on the left, and Z on the right, which turns out to be mostly determined via the part having the (larger) cross section \mathcal{A} . Furthermore, the flow rate \dot{U}_V (13) should stay small; this means that the (initial) liquid level difference $r' - r$ should be minimized, e.g., by

adjusting the cross sections or the reservoirs A, a, A' and a' , while the dominant flow resistance \mathcal{R} (12), as imposed by the isoradial segment of length $l_q = \delta z$ and cross section $A_q = a$, and scaling with the geometrical ratio $\delta z / a^2$, should be large. As the properties of the reagent are usually prescribed by the assay, an ancillary liquid possessing a high viscosity η' would also be beneficial to increase τ_β (14). Figure 3 shows the dependency of the resilience τ_β (14) on (left) the length δz , and (right) the cross section a of the Z -segment, which accounts for the biggest impact on the flow resistance \mathcal{R} (12) through $\mathcal{R}_q \propto \delta z / a^2$.

3.2.3 Design optimized for transport

By maximizing the quantities Δp_V (10) and τ_β (14) within the practical ranges of their input parameters $\{\gamma_k\}$ and their tolerances $\{\Delta\gamma_k\}$, the parametrized structure Γ can be algorithmically optimized to accomplish these design goals. Figure 4 shows (left) the layouts for the highest restoring pressure Δp_V (10), (center) the resilience τ_β (14), and (right) their product $\Delta p_V \cdot \tau_\beta$.

While the reasoning behind these designs is rather complicated, we point out some key characteristics of the optimization in Fig. 4. The left, pneumatically stabilized design shows a minimized gas volume above the reagent to raise the p_V (9) at the initial position $z = z$ (Fig. 1), thus preventing advancement of the phase interface during storage towards the DF. To still enable rotational actuation within the allowed frequency envelope, the gas volume above the ancillary liquid $V'(z = z)$ is kept noticeably larger. The resilience τ_β (14) in the central layout displaying open reservoirs is improved with

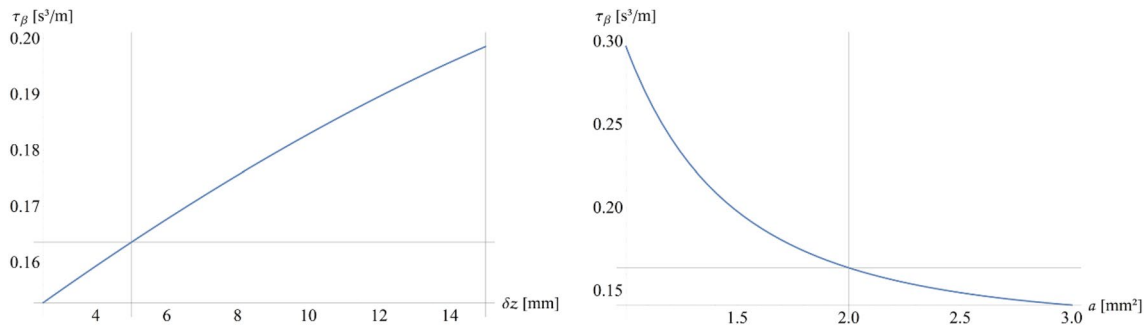


Fig. 3 Resilience quantified by τ_β (14) of the liquid distributions Λ and Λ' contained in the structure Γ as a function of (left) the length $l_q = \delta z$ of the isoradial segmented centered at z , and (right) its cross section $a_q = \omega$. As inferred from its definition (14), the resilience

τ_β steeply increases towards high flow resistance \mathcal{R} (12), i.e., with l_q/ω_q^2 . The gridlines mark the values when inserting default parameters (Table 1)

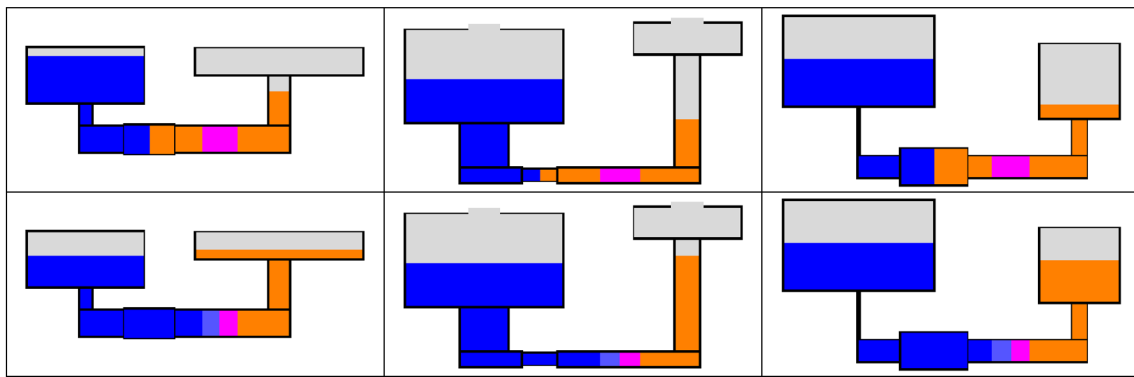


Fig. 4 Algorithmically optimized layouts Γ obtained with given design metrics for stabilizing the liquid–liquid interface at $z = z$ during transport. (Left) Pneumatic Δp_V (10): Both ports closed, (Center), Resilience τ_β (14): Both ports open, and (Right) Combination of

stabilization of pneumatics and resilience $\Delta p_V \cdot \tau_\beta$ with both ports closed, which finds the right balance between partially contradictory design guidelines

the high flow resistance \mathcal{R} (12), as imposed by the narrow section in the horizontal channel. The compromise design on the right-hand side of Fig. 4 features a tiny outer part of the radial channel on the reagent side to maintain a large Δr , and thus Δp_ω (4), so the counter pressure required for opening the DF at $z = z$ (Fig. 1) can still be provided.

4 Actuation

4.1 Pneumatic modes

In the case of the default scenario portrayed in Fig. 1, the inlets of the reservoirs for the aqueous reagent and the ancillary liquid are vented during rotation ($\omega > 0$), which can be interpreted as $V_0 \mapsto \infty$ and $V'_0 \mapsto \infty$ in (10), and thus $\Delta p_V \mapsto 0$ (10). So, as long as the centrifugally induced pressure head remains positive, i.e., $\Delta p_\omega > 0$ (5) for $z < z$, the meniscus will reach $z \geq z$, and thus wet and open the DF at the outlet. However, for centrifugo-pneumatic actuation, a critical spin rate

$$\Omega = \sqrt{\frac{p'_V - p_V}{\rho \bar{r} \Delta r - \rho' \bar{r}' \Delta r'}} \tag{15}$$

first needs to be surpassed, i.e., $\omega > \Omega$, before triggering reagent release. Here, the ambient pressure p_0 applies to open, and p_V and p'_V (9) to sealed ports. Such a finite $\Omega > 0$ (15) proves especially advantageous for multiplexed flow control (Ducrée 2021b, c).

As the default experimental parameters ρ, ρ', U, U', R and Γ (Table 1) are geared to result in $\Delta p_\omega = 0$ (5) at $z = \mathcal{Z}$, and thus $\Omega \mapsto \infty$, centrifugo-pneumatic actuation requires adjusting a subset of these variables. In general, the digital twin allows to calculate the changes required within the rather intricate correlation between the parameters $\rho, \rho', U, U', R, \Gamma$ and Ω in order realize certain design targets, e.g., a release threshold Ω (15) that is commensurate with a rotationally automated, multiplexed assay protocol. The example portrayed in Fig. 5 shows the scaling of the critical spin rate $\Omega/2\pi$ (15) with the ancillary volume $\chi \cdot U'$. Spindle speeds $\Omega/2\pi$ (15) within the experimentally feasible range smaller than 100 Hz only emerge below $\chi \approx 0.55$. It follows that, to make sure that the isoradial channel is always filled with the ancillary liquid, the cross sections \mathcal{A} and \mathcal{a} are both reduced by a factor of 3 with respect to the values in Table 1.

Note that Eq. (10) also discloses $\Delta p_V \propto p_0$. This scaling with the atmospheric pressure p_0 only affects the overall magnitude of Δp_V , but not the direction and ratio of the pneumatic pressures. We therefore refer to previous work on centrifugo-pneumatic valving where the impact and possible compensation of variation in the atmospheric pressure by weather, and particularly local altitude, have been examined in more detail (Ducrée 2021a, b, c, d).

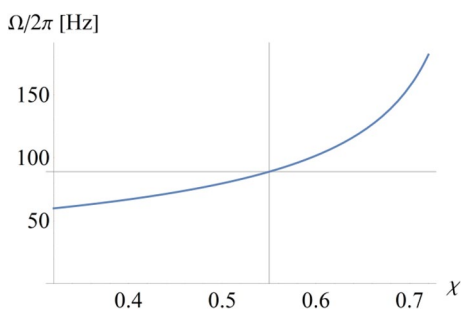


Fig. 5 Burst frequency $\Omega/2\pi$ required to establish $z = \mathcal{Z}$ when both inlet ports remain sealed during rotation when reducing the ancillary volume U' by a factor of χ . Towards $\chi \mapsto 1$, Ω reaches values that are way beyond the capabilities of typical LoAD instruments, thus effectively preventing release. Yet, spin rates below the practical upper limit $\omega/2\pi \approx 100$ Hz can be achieved below $\chi \approx 0.55$. Default parameters (Table 1) are employed, except that the cross sections \mathcal{A} and \mathcal{a} of the isoradial channel have been reduced by a factor of 3 to still assure its complete filling

The critical spin rate Ω (15), furthermore, determines the maximum (density) of the centrifugal field $f_\omega = \rho_{\text{part}} \cdot R_{\text{LUO}} \cdot \Omega^2$ that can be sustained by the reagent valve, e.g., while an LUO, for instance, plasma extraction, is simultaneously processed to separate blood cells of (relative) density ρ_{part} at $\omega < \Omega \pm M \cdot \Delta\Omega$.

4.2 Systematic volume losses

Due to evaporation or absorption at rates \dot{U} and \dot{U}' , liquid volumes U and U' may appreciably decline during storage over time periods T , typically lasting months up to a few years, by $\delta U = \dot{U} \cdot T$ and $\delta U' = \dot{U}' \cdot T$. Even for open inlet ports during rotation, the reduced volumes $U - \delta U$ and $U' - \delta U'$ may lead to $\Delta p_\omega(\rho, \rho', U - \delta U, U' - \delta U', R, \Gamma, \mathcal{Z}) < 0$ (5) (5), and thus cause valve malfunction by failure to dissolve the DF at $z = \mathcal{Z}$. (In addition, these volume losses δU and $\delta U'$ may also affect the outcome of quantitative bioassays.)

The main influence of the lost liquid volumes δU and $\delta U'$ on the density-weighted radial products $\bar{r} \Delta r$ and $\bar{r}' \Delta r'$ in the centrifugal equilibrium (6) manifests through $\Delta r = R - r$ and $\Delta r' = R - r'$ via $r(U, \delta U, A) = (U - \dot{U} \cdot T)/A$ and $r'(U', \delta U', A') = (U' - \dot{U}' \cdot T)/A'$. Enlarged cross sections A and A' thus reduce the effect of evaporation or other losses δU and $\delta U'$ of the reagent and ancillary phases at \dot{U} and \dot{U}' . Figure 6 shows that the prerequisite $\Delta p_\omega > 0$ for $z = \mathcal{Z}$ is assured for nearly 2.5 years at exemplary annual evaporation losses of 5% and 1% for the reagent and the ancillary liquid, respectively. This condition of a positive centrifugal pressure differential Δp_ω (10) also entails that sufficient liquid volumes U and U' remain available along all locations of the interface $z \leq z \leq \mathcal{Z}$, to eventually displace U_Δ (7) from

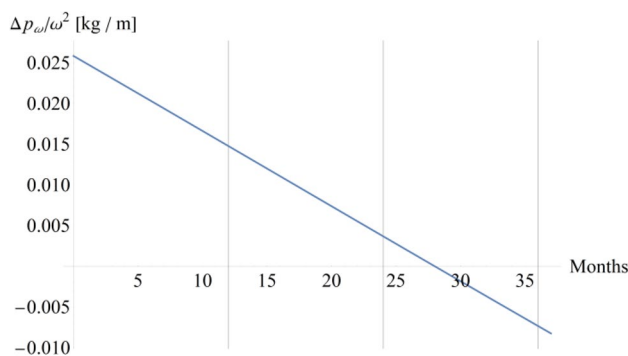


Fig. 6 Systematic reductions $\delta U = \dot{U} \cdot T$ and $\delta U' = \dot{U}' \cdot T$ of the originally loaded liquid volumes U and U' at rates \dot{U} and \dot{U}' , thus changing the centrifugal pressure balance p_ω/ω^2 (6) over a time period T . In this example, annual loss rates of \dot{U} and \dot{U}' of 5% and 1% are assumed, and $\dot{U} > \dot{U}'$ is compensated by loading 10% more reagent volume U . The curve uncovers that the opening condition $\Delta p_\omega/\omega^2 > 0$ at $z = \mathcal{Z}$ is assured beyond a typical minimum storage period of 24 months

the reagent side through the isoradial segment towards the ancillary reservoir.

If evaporation through the DF membrane turns out to be unacceptably high, its formulation ought to be altered, a coating applied, or its thickness enlarged. Note also that leaks in the assembly or permeation through the bulk material should be investigated. Moreover, even if the reagent valve still properly opens, the forwarded liquid volume might still be insufficient to actuate subsequent valves, e.g., by failing to generate enough centrifugal pressure head p_ω (4) for overcoming a critical frequency threshold, such as Ω (15).

4.3 Statistical tolerances

Consistent reagent release hinges upon $|\bar{z}(\rho, \rho', U, U', R, \Gamma, \Delta\rho, \Delta\rho', \Delta U, \Delta U', \Delta R, \Delta\Gamma) - Z| \leq M \cdot \Delta z (z = Z)$ in hydrostatic equilibrium (5) at $\omega > 0$. The standard deviation Δz (8) is affected by the unavoidable spreads $\{\Delta\gamma_k\}$ of the experimental input parameters $\{\gamma_k\}$, mainly within the geometrical dimensions $\Delta\Gamma$ and ΔU delineating the structure Γ , and the loaded liquid volumes U and U' , respectively.

The histogram in Fig. 7 displays the distribution of \bar{z} with a mean $\bar{z} = 19.97$ mm close to $Z = 20$ mm and a standard deviation $\Delta z = 4.02$ mm (8) as acquired from a Monte-Carlo simulation with 1000 runs using the default values and realistic tolerances Δd and Δw in vertical and lateral machining, and pipetting the liquid volumes ΔU and $\Delta U'$, as listed in Table 1. This digital-twin based Monte-Carlo method may be regarded as a virtualized manufacture and testing, which is very useful in view of the common paucity of physical devices throughout prototyping.

4.4 Gas enclosure

During priming or storage, bubbles may emerge from or between the two liquids, e.g., driven by the vapor pressure of the ancillary phase. For developing a semi-quantitative understanding of their influence on valving, we consider the case of a gas volume $V_{g,0}$ entrapped, after loading, at ambient pressure p_0 in the center of the isoradial z -segment. Upon reaching hydrostatic equilibrium during spinning at $\omega > 0$, its original volume $V_{g,0}$ is compressed to

$$V_g(\omega) = V_{g,0} \cdot \frac{p_0}{p_0 + p_\omega} = V_{g,0} \cdot \frac{p_0}{p_0 + \rho \cdot \bar{r} \Delta r \cdot \omega^2} \quad (16)$$

while now residing near $z = Z$. To still open the DF in presence of the entrapped gas, the liquid volumes U and U' need to be sized so that the meniscus at z was to shift by a further

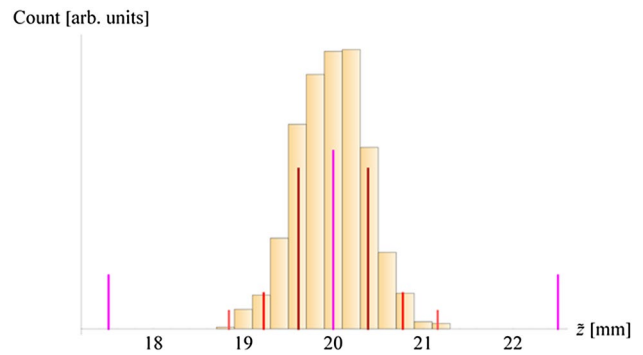


Fig. 7 Monte-Carlo simulation of the distribution of actual meniscus position \bar{z} when targeting $z = Z = 20$ mm at centrifugal equilibrium $\Delta p_\omega = 0$ found for the default parameters ρ, ρ', U, U', R and Γ while factoring in their respective tolerances $\Delta U, \Delta U'$ and $\Delta\Gamma$ (Table 1). After 1000 (time consuming) runs, the histogram features a mean position $\bar{z} = 19.99$ mm with a standard deviation $\Delta z = 0.387$ mm. The vertical lines indicate (magenta) the default center and limits of the DF at $z = Z$ and Z and $Z \pm 0.5$, respectively, and (red shades) $z = Z \pm M \cdot \Delta z$ with $M = \{1, 2, 3\}$ with the standard deviation Δz (8) of the \bar{z} -distribution

$0.5 \cdot V_g(\omega)/A$ (16) in the isoradial z -axis, compared to the absence of the bubble. (Alternatively, the position of the DF at Z can be appropriately adjusted to provide bubble tolerance.)

Assuming symmetrical displacement into each lateral reservoir (which is, strictly speaking, only the case for $\rho = \rho'$), the liquid levels r and r' in hydrostatic equilibrium (5) are lifted by about $0.5 \cdot V_g(\omega)/A$ and $0.5 \cdot V_g(\omega)/A'$ towards the center of rotation, respectively. The impact of such an entrapped gas bubble is assessed here in a back-of-the-envelope calculation; for this, we assume $V_0 = 1 \mu\text{l}$, $p_0 = p_{\text{std}}$, $v = \omega/2\pi = 25$ Hz and default values for the other parameters (Table 1), to arrive at $V \approx 0.9V_{g,0}$ and $\delta r \approx \delta r' \approx 1$ mm.

5 Refinements

To illustrate the very concept and potential of a digital twin for optimizing the long-term storage and release mechanism towards strategic design goals, we introduced a basic structure Γ (Fig. 1); this way, engineering objectives could be quantified and expressed by algebraic formulas without obfuscating the underlying mechanisms; moreover, these equations can be solved on reasonable time scales by commonly available computing resources.

Pegging the forward meniscus of the first introduced liquid by a minor capillary barrier, occasionally referred to as

phase guide, at $z = \mathcal{Z}$, is amongst many possible improvements. Trapping of an interstitial bubble after filling the second liquid may be prevented by an (initially) gas-permeable membrane, located near $z = \mathcal{Z}$, or a local outlet to be sealed after priming has been completed. Stiction of the progressing meniscus, e.g., caused by capillary pinning owing to manufacturing-related artefacts or dust, may be overcome by choosing a sufficiently elevated spin rate $\omega \gg 0$ for reaching hydrostatic equilibrium (5) at $z = \mathcal{Z}$.

In our own, naturally limited set of similar assay implementations (Lu et al. 2020; Mishra et al. 2020), we did not observe any adverse effect of the ancillary liquid on the bio-analytical performance. Yet, a general, blanket guarantee cannot be issued a priori. To avoid possible interference with the assay protocol, the immiscible ancillary liquid can be cleanly removed under prevalent laminar flow conditions through an additional, radially outer side pocket. Through centrifugal stratification, this reservoir can be designed to retain the entire volume of the higher-density ancillary liquid, while the released liquid reagent overflows towards the next stage. A corresponding structure has been proposed in the context of high-quality centrifugal separation of the plasma phase (Haeberle et al. 2006) (Czugala et al. 2013; Yao et al. 2021) or bands (Kinahan et al. 2016a) from whole blood.

Specific configurations of the reagent storage technique have been tested for premature opening upon possibly adverse conditions during storage, manual handling and transport. The valve proved to be stable, the main impact was evaporation, which was therefore included in the digital twin simulation (Fig. 6) (Lu et al. 2020; Mishra et al. 2020). It is assumed that a malicious, brute force approach would be required for inducing valve opening by deformation of the disc.

The permanently gas-filled parts of reservoirs may be placed at distal locations, as long as they are still pneumatically connected through conduits, e.g., to make efficient use of precious disc real estate required for multiplexed assay panels. The pneumatic seals may also be removed through a secondary mechanism, e.g., akin to venting procedures implemented for centrifugo-pneumatic valves based on mechanical (Kinahan et al. 2016b), laser- (García-Cordero et al. 2010; Mishra et al. 2018) or pneumatic (Keller et al. 2015; Hess et al. 2019; Kinahan et al. 2016c, 2018; Godino et al. 2012, 2013; Schwemmer et al. 2015a; Zhao et al. 2015; Zehnle et al. 2015; Ducrée 2021c; Mishra et al. 2018; Gorkin et al. 2010b, 2011; Mark et al. 2008, 2009b) principles.

6 Summary and outlook

6.1 Summary

A novel technology has been introduced for Lab-on-a-Disc systems, which offers a physical evaporation barrier and stabilization of liquid distributions during long-term storage, transport, and handling. Initially protected by an immiscible ancillary liquid, the aqueous reagent contacts a dissolvable film by centrifugal displacement. The convoluted interdependencies governing the operational principle over its multiparameter space have been modelled to characterize system robustness and behavior *in silico*. The resulting digital twin further enables computational design optimization towards given performance objectives within practically achievable regimes of the experimental input parameters and their tolerances. In addition, systematic volume losses, e.g., through evaporation during storage, artefacts such as enclosed gas bubbles, and statistical deviations in the governing parameters can be factored in, thus permitting algorithmic enhancement of the operational robustness of the valving mechanism.

6.2 Outlook

Evidently, the work presented only represents a blueprint for setting up digital twins to efficiently characterize and improve other functional elements of (centrifugal) microfluidic Lab-on-a-Disc systems. Its simplified representation of the valving structure by cuboidal elements can be significantly refined to optimize flow, e.g., by curved contours of the compartments, their inclination with respect to the radial orientation, and fins to guide the relocation of liquids and gases. Similar to the entrapped bubble, further parasitic effects observed during experimental testing, and additional elements of the layout can be included in the digital twin. Such enhancements will require a more complex computational fluid dynamic (CFD) simulation, which should also include inertia of the liquid and elastic components, like the sealing membranes, which may bend or even yield under pressure.

It is well known that tests with real systems will show effects that are not included in the digital-twin modelling. So, it is well expected that experimental validation will remain a substantial tool for arriving at a product. Nevertheless, in particular during the early stage of development where manufacturing and testing are mostly manual, only smaller numbers of fluidic chips are available, which usually precludes collecting sufficient statistics for proper device

performance and reliability analysis. Extensive experimental validation of a wide spectrum of use cases, and sophistication of the rudimentary digital twin model, by the scientific community is highly encouraged.

The digital twin presented in this work can then markedly expedite the design iteration of microfluidic systems by providing virtual prototyping and testing. Such a tool hence empowers failure mode and effects analysis (FMEA) regarding unavoidable tolerances, and in silico optimization of the layout for given design targets. Adding similar programs for simulating manufacturing and biochemical processes would also be desirable to combine with the digital twin for fluidics presented here.

On the bigger picture, the digital twin approach can boost microfluidic industries by standardization (Heeren 2012; Stavis 2012; Reyes et al. 2021), interpreted in a way that validated boundary conditions issued by foundries can be incorporated in computational design software to guarantee manufacturability, reliability and targetted performance within given cost limits. Moreover, the digital twin modelling published here, in tandem with simultaneously evolving, exponential technologies such as artificial intelligence (AI) and digital manufacture in an increasingly virtualized "metaverse" (Metaverse 2021; Meta 2021), lends itself for open platform concepts which can leverage crowdsourcing of brains, hands, infrastructure and equipment, e.g., coordinated by the rapidly emerging, decentralized blockchain

technology (Ducrée et al. 2020a, b, 2021; Ducrée 2020, 2021e).

Appendix

The default parameters of the basic structure Γ in Fig. 1 are listed in Table 1. The tolerances in vertical and lateral dimensions are $\Delta d = 30 \mu\text{m}$ and $\Delta w = 20 \mu\text{m}$, respectively. The minimum wall thickness between fluidic cavities is set to 1 mm to account for scale-up of production by common injection molding schemes, and to provide adequate bonding surface. The properties of water and "FC-72" (3 M™ Fluorinert™ Electronic Liquid FC-72) representing an aqueous reagent and an immiscible ancillary liquid (at 25 °C) are used. The volume of the ancillary fluid U' is chosen to settle $z = \mathcal{Z}$ at $\omega > 0$ (for both reservoirs open). For the definition of liquid volumes, $\Delta U = \Delta U' = 100 \text{ nl}$ are assumed, and a minimum gap δH between the filling level and the seal is implemented to facilitate proper experimental loading. Fluctuations in p_0 with respect to the standard atmospheric pressure p_{std} are limited to the range of typical weather conditions, i.e., about 4%; the impact of the local altitude on p_0 is more pronounced when operating the Load in mountainous regions. The effect of variances in $\varrho, \varrho', \mathcal{Z}, \delta\mathcal{Z}, \mathcal{L}$ and R on the meniscus position z is assumed to be negligible.

Table 1 Default dimensions and boundary conditions for experimental parameters of the basic valving structure Γ (Fig. 1)

Isoradial channel	$R = 30 \text{ mm}$	$\mathcal{L} = 30 \text{ mm}$	$\mathcal{H} = 3 \text{ mm}$
Isoradial \mathcal{Z} -Segment	$z = 10 \text{ mm}$	$\delta z = 5 \text{ mm}$	$h = 2 \text{ mm}$
DF Region	$\mathcal{Z} = 15 \text{ mm}$	$\delta\mathcal{Z} = 5 \text{ mm}$	
Cross sections (depth \times width)	$A = 1 \text{ mm} \times 10 \text{ mm}$ $a = 1 \text{ mm} \times 5 \text{ mm}$	$A' = 1 \text{ mm} \times 10 \text{ mm}$ $a' = 1 \text{ mm} \times 4.5 \text{ mm}$	$\mathcal{A} = 1 \text{ mm} \times 3 \text{ mm}$ $\mathcal{a} = 1 \text{ mm} \times 2 \text{ mm}$
Depths	$D = d = 1 \text{ mm}$	$D' = d' = 1 \text{ mm}$	$\mathcal{D} = \mathcal{d} = 1 \text{ mm}$
Reservoir heights	$H = 15 \text{ mm}$ $h = 5 \text{ mm}$	$H' = 10 \text{ mm}$ $h' = 2.5 \text{ mm}$	
Minimum dimensions	Vertical $\geq 300 \mu\text{m}$	Lateral $\geq 200 \mu\text{m}$	Wall Thickness $\geq 1 \text{ mm}$
Structurable area:	$R_{\text{min}} = 7.5 \text{ mm}$	$R_{\text{max}} = 55 \text{ mm}$	
Geom. tolerances	Vertical: $30 \mu\text{m}$	Lateral: $20 \mu\text{m}$	
Liquid volumes	$U = 160 \mu\text{l}$	$U' \approx 60.68 \mu\text{l}$	$\Delta U = \Delta U' = 100 \text{ nl}$
Minimum filling gap	$\delta H = \delta H' = 1 \text{ mm}$		
Liquid densities	$\varrho = 997 \text{ kg} \cdot \text{m}^{-3}$	$\varrho' = 1680 \text{ kg} \cdot \text{m}^{-3}$	
Liquid viscosities	$\eta = 1.0016 \text{ mPa} \cdot \text{s}$	$\eta' = 0.64 \text{ mPa} \cdot \text{s}$	
Ambient pressure	$p_0 = p_{\text{std}} = 1013.25 \text{ hPa}$		

Funding Open Access funding provided by the IReL Consortium.

Open Access This article is licensed under a Creative Commons Attribution 4.0 International License, which permits use, sharing, adaptation, distribution and reproduction in any medium or format, as long as you give appropriate credit to the original author(s) and the source, provide a link to the Creative Commons licence, and indicate if changes were made. The images or other third party material in this article are included in the article's Creative Commons licence, unless indicated otherwise in a credit line to the material. If material is not included in the article's Creative Commons licence and your intended use is not permitted by statutory regulation or exceeds the permitted use, you will need to obtain permission directly from the copyright holder. To view a copy of this licence, visit <http://creativecommons.org/licenses/by/4.0/>.

References

- Abaxis (Piccolo Express). Available on: <https://www.abaxis.com/>. Accessed: 14 Jun 2021
- Abi-Samra K, Clime L, Kong L, Gorkin R, Kim TH, Cho YK, Madou M (2011a) Thermo-pneumatic pumping in centrifugal microfluidic platforms. *Microfluid Nanofluid* 11:643–652. <https://doi.org/10.1007/s10404-011-0830-5>
- Abi-Samra K, Hanson R, Madou M, Gorkin RA (2011b) Infrared controlled waxes for liquid handling and storage on a CD-microfluidic platform. *Lab Chip* 11:723–726. <https://doi.org/10.1039/c0lc00160k>
- Aeinehvand MM, Magaña P, Aeinehvand MS, Aguilar O, Madou MJ, Martínez-Chapa SO (2017) Ultra-rapid and low-cost fabrication of centrifugal microfluidic platforms with active mechanical valves. *RSC Adv* 7:55400–55407. <https://doi.org/10.1039/c7ra11532f>
- Aeinehvand MM, Ibrahim F, Al-Faqheri W, Joseph K, Madou MJ (2018) Recent advances in the development of micropumps, microvalves and micromixers and the integration of carbon electrodes on centrifugal microfluidic platforms. *Int J Nanotechnol* 15:53–68. <https://doi.org/10.1504/IJNT.2018.089559>
- Aeinehvand MM, Weber L, Jiménez M, Palermo A, Bauer M, Loeffler FF, Ibrahim F, Breitling F, Korvink J, Madou M, Mager D, Martínez-Chapa SO (2019) Elastic reversible valves on centrifugal microfluidic platforms. *Lab Chip* 19:1090–1100. <https://doi.org/10.1039/C8LC00849C>
- Al-Faqheri W, Ibrahim F, Thio THG, Moebius J, Joseph K, Arof H, Madou M (2013) Vacuum/compression valving (VCV) using paraffin-wax on a centrifugal microfluidic CD platform. *PLoS ONE*. <https://doi.org/10.1371/journal.pone.0058523>
- Andersson P, Jesson G, Kylberg G, Ekstrand G, Thorsen G (2007) Parallel nanoliter microfluidic analysis system. *Anal Chem* 79:4022–4030. <https://doi.org/10.1021/ac061692y>
- Auroux P-A, Iossifidis D, Reyes DR, Manz A (2002) Micro total analysis systems. 2. Analytical standard operations and applications. *Anal Chem* 74:2637–2652. <https://doi.org/10.1021/ac020239t>
- Azimi-Boulali J, Madadelahi M, Madou MJ, Martínez-Chapa SO (2020) Droplet and particle generation on centrifugal microfluidic platforms: a review. *Micromachines*. <https://doi.org/10.3390/mi11060603>
- Baier T, Hansen-Hagge TE, Gransee R, Crombé A, Schmahl S, Paulus C, Drese KS, Keegan H, Martin C, O'Leary JJ, Furuberg L, Solli L, Grønn P, Falang IM, Karlgård A, Gulliksen A, Karlsen F (2009) Hands-free sample preparation platform for nucleic acid analysis. *Lab Chip* 9(23):3399
- Brassard D, Geissler M, Descarreaux M, Tremblay D, Daoud J, Clime L, Mounier M, Charlebois D, Veres T (2019) Extraction of nucleic acids from blood: unveiling the potential of active pneumatic pumping in centrifugal microfluidics for integration and automation of sample preparation processes. *Lab Chip* 19:1941–1952. <https://doi.org/10.1039/c9lc00276f>
- Brennan D, Coughlan H, Clancy E, Dimov N, Barry T, Kinahan D, Ducrée J, Smith TJ, Galvin P (2017) Development of an on-disc isothermal in vitro amplification and detection of bacterial RNA. *Sens Actuat b: Chem* 239:235–242. <https://doi.org/10.1016/j.snb.2016.08.018>
- Burger R, Amato L, Boisen A (2016) Detection methods for centrifugal microfluidic platforms. *Biosens Bioelectron* 76:54–67. <https://doi.org/10.1016/j.bios.2015.06.075>
- Burger R, Kinahan D, Cayron H, Reis N, Garcia da Fonseca J, Ducrée J (2020) Siphon-induced droplet break-off for enhanced mixing on a centrifugal platform. *Inventions*. <https://doi.org/10.3390/inventions5010001>
- Clime L, Brassard D, Geissler M, Veres T (2015) Active pneumatic control of centrifugal microfluidic flows for lab-on-a-chip applications. *Lab Chip* 15:2400–2411. <https://doi.org/10.1039/c4lc01490a>
- Clime L, Daoud J, Brassard D, Malic L, Geissler M, Veres T (2019) Active pumping and control of flows in centrifugal microfluidics. *Microfluid Nanofluid*. <https://doi.org/10.1007/s10404-019-2198-x>
- Czilwik G, Vashist SK, Klein V, Buderer A, Roth G, von Stetten F, Zengerle R, Mark D (2015) Magnetic chemiluminescent immunoassay for human C-reactive protein on the centrifugal microfluidics platform. *RSC Adv* 5(76):61906–61912
- Czugala M, Maher D, Collins F, Burger R, Hopfgartner F, Yang Y, Zhaou J, Ducrée J, Smeaton A, Fraser KJ, Benito-Lopez F, Diamond D (2013) CMAS: fully integrated portable centrifugal microfluidic analysis system for on-site colorimetric analysis. *RSC Adv* 3:15928–15938. <https://doi.org/10.1039/c3ra42975j>
- Czurratis D, Beyl Y, Grimm A, Brettschneider T, Zinobor S, Lärmer F, Zengerle R (2015) Liquids on-chip: direct storage and release employing micro-perforated vapor barrier films. *Lab Chip* 15:2887–2895. <https://doi.org/10.1039/c5lc00510h>
- Delgado SMT, Kinahan DJ, Sandoval FS, Julius LAN, Kilcawley NA, Ducrée J, Mager D (2016) Fully automated chemiluminescence detection using an electrified-Lab-on-a-Disc (eLoad) platform. *Lab Chip* 16:4002–4011. <https://doi.org/10.1039/c6lc00973e>
- Delgado SMT, Kinahan DJ, Julius LAN, Mallette A, Ardila DS, Mishra R, Miyazaki CM, Korvink JG, Ducrée J, Mager D (2018) Wirelessly powered and remotely controlled valve-array for highly multiplexed analytical assay automation on a centrifugal microfluidic platform. *Biosens Bioelectron* 109:214–223. <https://doi.org/10.1016/j.bios.2018.03.012>
- Deng J, Jiang X (2019) Advances in reagents storage and release in self-contained point-of-care devices. *Adv Mater Technol* 4:1800625. <https://doi.org/10.1002/admt.201800625>
- Digital Twin. 2021; Available on: https://en.wikipedia.org/wiki/Digital_twin. 25 May 2021
- Dimov N, Gaughran J, McAuley D, Boyle D, Kinahan DJ, Ducrée J (2014) Centrifugally automated solid-phase purification of RNA. In: 2014 IEEE 27th International Conference on Micro Electro Mechanical Systems (MEMS), 2014, pp 260–263 <https://doi.org/10.1109/MEMSYS.2014.6765625>
- Ducrée J (2019) Efficient development of integrated Lab-On-A-Chip systems featuring operational robustness and manufacturability. *Micromachines* 10:12. <https://doi.org/10.3390/mi10120886>
- Ducrée J (2020) Research—a blockchain of knowledge? *Blockchain Res Appl* 1:100005. <https://doi.org/10.1016/j.bcra.2020.100005>
- Ducrée J (2021a) Design optimization of centrifugal microfluidic “Lab-on-a-Disc” systems towards fluidic larger-scale integration. *Appl Sci* 11:5839. <https://doi.org/10.3390/app11135839>

- Ducrée J (2021b) Systematic review of centrifugal valving based on digital twin modelling towards highly integrated Lab-on-a-Disc systems. *Nat Microsyst Nanoeng*. <https://doi.org/10.1038/s41378-021-00317-3>
- Ducrée J (2021c) Secure air traffic control at the hub of multiplexing on the centrifugo-pneumatic Lab-on-a-Disc platform. *Micromachines* 12:700. <https://doi.org/10.3390/mi12060700>
- Ducrée J (2021d) Anti-counterfeit technologies for microfluidic “Lab-on-a-Disc” systems. *Sens Actuat A Phys*. <https://doi.org/10.20944/preprints202107.0443.v1>
- Ducrée J (2021e) Digital twins – enabling oracles for efficient crowdsourcing of research & technology development through blockchain. *Sci Rep*. <https://doi.org/10.20944/preprints202110.0148.v1>
- Ducrée J, Brenner T, Haerberle S, Glatzel T, Zengerle R (2006a) Multilamination of flows in planar networks of rotating microchannels. *Microfluid Nanofluid* 2:78–84. <https://doi.org/10.1007/s10404-005-0056-5>
- Ducrée J, Haerberle S, Brenner T, Glatzel T, Zengerle R (2006b) Patterning of flow and mixing in rotating radial microchannels. *Microfluid Nanofluid* 2:97–105. <https://doi.org/10.1007/s10404-005-0049-4>
- Ducrée J, Haerberle S, Lutz S, Pausch S, von Stetten F, Zengerle R (2007) The centrifugal microfluidic bio-disk platform. *J Micro-mech Microeng* 17:S103–S115. <https://doi.org/10.1088/0960-1317/17/7/S07>
- Ducrée J, Gravitt M, Walshe R, Bartling S, Etzrodt M, Harrington T (2020a) Open platform concept for blockchain-enabled crowdsourcing of technology development and supply chains. *Front Blockchain* 3:386525. <https://doi.org/10.3389/fbloc.2020.586525>
- Ducrée J, Etzrodt M, Gordijn B, Gravitt M, Bartling S, Walshe R, Harrington T (2020b) Blockchain for organising effective grass-roots actions on a global commons: saving the planet. *Front Blockchain* 3:33. <https://doi.org/10.3389/fbloc.2020.00033>
- Ducrée J, Etzrodt M, Bartling S, Walshe R, Harrington T, Wittek N, Posth S, Ionita KWA, Prinz W, Kogias D, Paixão T, Peterfi I, Lawton J (2021) Unchaining collective intelligence for science, research and technology development by blockchain-boosted community participation. *Front Blockchain*. <https://doi.org/10.3389/fbloc.2021.631648>
- Duffy DC, Gillis HL, Lin J, Sheppard NF, Kellogg GJ (1999) Microfabricated centrifugal microfluidic systems: characterization and multiple enzymatic assays. *Anal Chem* 71:4669–4678. <https://doi.org/10.1021/ac990682c>
- Eker B, Temiz Y, Delamarche E (2014) Heterogeneous integration of gels into microfluidics using a mesh carrier. *Biomed Microdev* 16:829–835. <https://doi.org/10.1007/s10544-014-9886-9>
- García-Cordero JL, Benito-Lopez F, Diamond D, Ducrée J, Ricco AJ (2009) Low-cost microfluidic single-use valves and on-board reagent storage using laser-printer technology. In: *IEEE 22nd International Conference on Micro Electro Mechanical Systems (MEMS 2009)*, pp 439–442. <https://doi.org/10.1109/Memsys.2009.4805413>
- García-Cordero JL, Kurzbuch D, Benito-Lopez F, Diamond D, Lee LP, Ricco AJ (2010) Optically addressable single-use microfluidic valves by laser printer lithography. *Lab Chip* 10:2680–2687. <https://doi.org/10.1039/c004980h>
- Gaughran J, Boyle D, Murphy J, Kelly R, Ducrée J (2016) Phase-selective graphene oxide membranes for advanced microfluidic flow control. *Microsyst Nanoeng* 2:16008. <https://doi.org/10.1038/micronano.2016.8>
- Gijs MAM, Lacharme F, Lehmann U (2010) Microfluidic applications of magnetic particles for biological analysis and catalysis. *Chem Rev* 110:1518–1563. <https://doi.org/10.1021/cr9001929>
- Godino N, Gorkin R, Linares AV, Burger R, Ducrée J (2012) A Centrifugo-Pneumatic Cascade for Fully Integrated and Multiplexed Biological Analysis. In: *2012 IEEE 25th International Conference on Micro Electro Mechanical Systems (MEMS)*. 2012: Paris, France. <https://doi.org/10.1109/MEMSYS.2012.6170352>
- Godino N, Gorkin R 3rd, Linares AV, Burger R, Ducrée J (2013) Comprehensive integration of homogeneous bioassays via centrifugo-pneumatic cascading. *Lab Chip* 13:685–694. <https://doi.org/10.1039/c2lc40722a>
- Gorkin R, Park J, Siegrist J, Amasia M, Lee BS, Park JM, Kim J, Kim H, Madou M, Cho YK (2010a) Centrifugal microfluidics for biomedical applications. *Lab Chip* 10:1758–1773. <https://doi.org/10.1039/b924109d>
- Gorkin R, Clime L, Madou M, Kido H (2010b) Pneumatic pumping in centrifugal microfluidic platforms. *Microfluid Nanofluid* 9:541–549. <https://doi.org/10.1007/s10404-010-0571-x>
- Gorkin R, Nwankire C, Siegrist J, Burger R, Gaughran J, Ducrée J (2011) Rotationally controlled centrifugo-pneumatic valving utilizing dissolvable films. In: *2011 16th International Solid-State Sensors, Actuators and Microsystems Conference*. pp 1276–1279. <https://doi.org/10.1109/transducers.2011.5969448>
- Gorkin R, Nwankire CE, Gaughran J, Zhang X, Donohoe GG, Rook M, Okennedy R, Ducrée J (2012) Centrifugo-pneumatic valving utilizing dissolvable films. *Lab Chip* 12:2894–2902. <https://doi.org/10.1039/c2lc20973j>
- Grieves M, Vickers J (2017) Digital twin: mitigating unpredictable, undesirable emergent behavior in complex systems. In: Kahlen F-J, Flumerfelt S, Alves A (eds) *Transdisciplinary perspectives on complex systems: new findings and approaches*. Springer International Publishing, Cham, pp 85–113
- Grumann M, Geipel A, Riegger L, Zengerle R, Ducrée J (2004) Magneto-hydrodynamic micromixing for centrifugal lab-on-a-disk platforms. In: *Micro Total Analysis Systems 2004, Vol 1*, pp 593–595
- Grumann M, Geipel A, Riegger L, Zengerle R, Ducrée J (2005) Batch-mode mixing on centrifugal microfluidic platforms. *Lab Chip* 5:560–565. <https://doi.org/10.1039/b418253g>
- Gyros Protein Technologies. Available on: <https://www.gyrosproteintechologies.com/>. Accessed: 14 Jun 2021
- Haerberle S, Brenner T, Zengerle R, Ducrée J (2006) Centrifugal extraction of plasma from whole blood on a rotating disk. *Lab Chip* 6:776–781. <https://doi.org/10.1039/b604145k>
- Haerberle S, Zengerle R, Ducrée J (2007) Centrifugal generation and manipulation of droplet emulsions. *Microfluid Nanofluid* 3:65–75. <https://doi.org/10.1007/s10404-006-0106-7>
- Haerberle S, Naegele L, Burger R, Von Stetten F, Zengerle R, Ducrée J (2008) Alginate bead fabrication and encapsulation of living cells under centrifugally induced artificial gravity conditions. *J Microencapsul* 25:267–274. <https://doi.org/10.1080/02652040801954333>
- Henderson BD, Kinahan DJ, Rio J, Mishra R, King D, Torres-Delgado SM, Mager D, Korvink JG, Ducrée J (2021) Siphon-controlled automation on a lab-on-a-disc using event-triggered dissolvable film valves. *Biosensors*. <https://doi.org/10.3390/1108103>
- Hess JF, Zehnle S, Juelg P, Hutzenlaub T, Zengerle R, Paust N (2019) Review on pneumatic operations in centrifugal microfluidics. *Lab Chip* 19:3745–3770. <https://doi.org/10.1039/C9LC00441F>
- Hin S, Paust N, Keller M, Rombach M, Strohmeier O, Zengerle R, Mitsakakis K (2018) Temperature change rate actuated bubble mixing for homogeneous rehydration of dry pre-stored reagents in centrifugal microfluidics. *Lab Chip* 18:362–370. <https://doi.org/10.1039/c7lc01249g>
- Hoffmann J, Mark D, Lutz S, Zengerle R, Von Stetten F (2010) Pre-storage of liquid reagents in glass ampoules for DNA extraction on a fully integrated lab-on-a-chip cartridge. *Lab Chip* 10:1480. <https://doi.org/10.1039/b926139g>

- Homann AR, Niebling L, Zehnle S, Beutler M, Delamotte L, Rothmund M-C, Czurratis D, Beller K-D, Zengerle R, Hoffmann H, Paust N (2021) A microfluidic cartridge for fast and accurate diagnosis of Mycobacterium tuberculosis infections on standard laboratory equipment. *Lab Chip*. <https://doi.org/10.1039/d1lc00035g>
- Inganas M, Derand H, Eckersten A, Ekstrand G, Honerud AK, Jeson G, Thorsen G, Soderman T, Andersson P (2005) Integrated microfluidic compact disc device with potential use in both centralized and point-of-care laboratory settings. *Clin Chem* 51:1985–1987. <https://doi.org/10.1373/clinchem.2005.053181>
- Janasek D, Franzke J, Manz A (2006) Scaling and the design of miniaturized chemical-analysis systems. *Nature* 442:374–380. <https://doi.org/10.1038/nature05059>
- Karle M, Miwa J, Roth G, Zengerle R, von Stetten F (2009) A novel microfluidic platform for continuous DNA extraction and purification using laminar flow magnetophoresis. In: IEEE 22nd International Conference on Micro Electro Mechanical Systems (MEMS 2009), 2009, pp 276–279 <https://doi.org/10.1109/Memsys.2009.4805372>
- Kazemzadeh A, Eriksson A, Madou M, Russom A (2019) A microdispenser for long-term storage and controlled release of liquids. *Nat Commun*. <https://doi.org/10.1038/s41467-018-08091-z>
- Keller M, Wadle S, Paust N, Dreesen L, Nuese C, Strohmeyer O, Zengerle R, von Stetten F (2015) Centrifugo-thermopneumatic fluid control for valving and aliquoting applied to multiplex real-time PCR on off-the-shelf centrifugal thermocycler. *RSC Adv* 5:89603–89611. <https://doi.org/10.1039/c5ra16095b>
- Kido H, Micic M, Smith D, Zoval J, Norton J, Madou M (2007) A novel, compact disk-like centrifugal microfluidics system for cell lysis and sample homogenization. *Colloids Surf B Biointerfaces* 58:44–51. <https://doi.org/10.1016/j.colsurfb.2007.03.015>
- Kim TH, Abi-Samra K, Sunkara V, Park DK, Amasia M, Kim N, Kim J, Kim H, Madou M, Cho YK (2013) Flow-enhanced electrochemical immunosensors on centrifugal microfluidic platforms. *Lab Chip* 13(18):3747–3754. <https://doi.org/10.1039/c3lc50374g>
- Kinahan DJ, Kearney SM, Dimov N, Glynn MT, Ducrée J (2014) Event-triggered logical flow control for comprehensive process integration of multi-step assays on centrifugal microfluidic platforms. *Lab Chip* 14:2249–2258. <https://doi.org/10.1039/c4lc00380b>
- Kinahan DJ, Kearney SM, Faneuil OP, Glynn MT, Dimov N, Ducrée J (2015) Paper imbibition for timing of multi-step liquid handling protocols on event-triggered centrifugal microfluidic lab-on-a-disc platforms. *RSC Adv* 5:1818–1826. <https://doi.org/10.1039/c4ra14887h>
- Kinahan DJ, Kearney SM, Kilcawley NA, Early PL, Glynn MT, Ducrée J (2016a) Density-gradient mediated band extraction of leukocytes from whole blood using centrifugo-pneumatic siphon valving on centrifugal microfluidic discs. *PLoS ONE* 11:e0155545. <https://doi.org/10.1371/journal.pone.0155545>
- Kinahan DJ, Early PL, Vembadi A, MacNamara E, Kilcawley NA, Glennon T, Diamond D, Brabazon D, Ducrée J (2016b) Xurography actuated valving for centrifugal flow control. *Lab Chip* 16:3454–3459. <https://doi.org/10.1039/c6lc00568c>
- Kinahan DJ, Renou M, Kurzbuch D, Kilcawley NA, Bailey E, Glynn MT, McDonagh C, Ducrée J (2016c) Baking powder actuated centrifugo-pneumatic valving for automation of multi-step bioassays. *Micromachines*. <https://doi.org/10.3390/mi7100175>
- Kinahan DJ, Delgado SM, Julius LAN, Mallette A, Saenz-Ardila D, Mishra R, Miyazaki CM, Korvink J, Mager D, Ducrée J (2018) Wireless closed-loop control of centrifugo-pneumatic valving towards large-scale microfluidic process integration. In: 2018 IEEE Micro Electro Mechanical Systems (MEMS), Belfast, Northern Ireland, pp 1213–1216 <https://doi.org/10.1109/MEMSYS.2018.8346781>
- Kloke A, Fiebach AR, Zhang S, Drechsel L, Niekrawietz S, Hoehl MM, Kneusel R, Panthel K, Steigert J, Von Stetten F, Zengerle R, Paust N (2014) The LabTube—a novel microfluidic platform for assay automation in laboratory centrifuges. *Lab Chip* 14:1527–1537. <https://doi.org/10.1039/c3lc51261d>
- Kong LX, Parate K, Abi-Samra K, Madou M (2015) Multifunctional wax valves for liquid handling and incubation on a microfluidic CD. *Microfluid Nanofluid* 18:1031–1037. <https://doi.org/10.1007/s10404-014-1492-x>
- Kong LX, Perebikovsky A, Moebius J, Kulinsky L, Madou M (2016a) Lab-on-a-CD: a fully integrated molecular diagnostic system. *J Assoc Lab Autom* 21:323–355. <https://doi.org/10.1177/2211068215588456>
- Kong LX, Perebikovsky A, Moebius J, Kulinsky L, Madou M (2016b) Lab-on-a-CD. *J Lab Autom* 21:323–355. <https://doi.org/10.1177/2211068215588456>
- Krauss ST, Woolf MS, Hadley KC, Collins NM, Nauman AQ, Landers JP (2019) Centrifugal microfluidic devices using low-volume reagent storage and inward fluid displacement for presumptive drug detection. *Sens Actuat B Chem* 284:704–710. <https://doi.org/10.1016/j.snb.2018.12.113>
- Li N, Lu Y, Cheng J, Xu Y (2020) A self-contained and fully integrated fluidic cassette system for multiplex nucleic acid detection of bacteriuria. *Lab Chip* 20:384–393. <https://doi.org/10.1039/c9lc00994a>
- Liu Q, Wu C, Cai H, Hu N, Zhou J, Wang P (2014) Cell-based biosensors and their application in biomedicine. *Chem Rev* 114:6423–6461. <https://doi.org/10.1021/cr2003129>
- Lu Y, Mishra R, McAuley D, Boyle D, Ducrée J (2020) Reliable liquid reagent storage and rotational recovery for centrifugal sample-to-answer automation. In: Lu SLGaH (ed) Proceedings of the 24th International Conference on Miniaturized Systems for Chemistry and Life Sciences (μ TAS 2020), October 04–08, The Chemical and Biological Microsystems Society (CBMS): Virtual, pp 134–135
- Lutz S, Mark D, Roth G, Zengerle R, von Stetten F (2011) Centrifugal microfluidic platforms for molecular diagnostics. *Clin Chem Lab Med* 49:S608–S608
- Madadelahi M, Acosta-Soto LF, Hosseini S, Martinez-Chapa SO, Madou MJ (2020) Mathematical modeling and computational analysis of centrifugal microfluidic platforms: a review. *Lab Chip* 20:1318–1357. <https://doi.org/10.1039/c9lc00775j>
- Madou MJ, Kellogg GJ (1998) The LabCD (TM): a centrifuge-based microfluidic platform for diagnostics. *Syst Technol Clin Diagn Drug Discov* 3259:80–93. <https://doi.org/10.1117/12.307314>
- Maguire I, O’Kennedy R, Ducrée J, Regan F (2018) A review of centrifugal microfluidics in environmental monitoring. *Anal Methods* 10:1497–1515. <https://doi.org/10.1039/c8ay00361k>
- Manz A, Graber N, Widmer HM (1990) Miniaturized total chemical analysis systems: a novel concept for chemical sensing. *Sens Actuat B Chem* 1(244):248. [https://doi.org/10.1016/0925-4005\(90\)80209-I](https://doi.org/10.1016/0925-4005(90)80209-I)
- Margell RBMLJ, Hjort K, Schweitz J-Å (2008) On-chip liquid storage and dispensing for lab-on-a-chip applications. *J Micromech Microeng* 18:075036. <https://doi.org/10.1088/0960-1317/18>
- Mark D, Haeberle S, Metz T, Lutz S, Ducrée J, Zengerle R, von Stetten F (2008) Aliquoting structure for centrifugal microfluidics based on a new pneumatic valve. In: MEMS 2008: 21st IEEE International Conference on Micro Electro Mechanical Systems, Technical Digest, 2008, pp 611–614. <https://doi.org/10.1109/MEMSYS.2008.4443730>

- Mark D, Haeberle S, Zengerle R, Ducrée J, Vladisavljevic GT (2009a) Manufacture of chitosan microbeads using centrifugally driven flow of gel-forming solutions through a polymeric micronozzle. *J Colloid Interface Sci* 336:634–641. <https://doi.org/10.1016/j.jcis.2009.04.029>
- Mark D, Metz T, Haeberle S, Lutz S, Ducrée J, Zengerle R, von Stetten F (2009b) Centrifugo-pneumatic valve for metering of highly wetting liquids on centrifugal microfluidic platforms. *Lab Chip* 9:3599–3603. <https://doi.org/10.1039/b914415c>
- Marr B (2017) What is digital twin technology—and why is it so important? 2017 Published: 06/03/2017; Available on: <https://www.forbes.com/sites/bernardmarr/2017/03/06/what-is-digital-twin-technology-and-why-is-it-so-important/>. 25 May 2021
- Mauk M, Song J, Bau HH, Gross R, Bushman FD, Collman RG, Liu C (2017) Miniaturized devices for point of care molecular detection of HIV. *Lab Chip* 17:382–394. <https://doi.org/10.1039/c6lc01239f>
- Meta. 2021 Available on: <https://www.meta.com>. Accessed 08 Nov 2021
- Metaverse (2021) Available on: <https://en.wikipedia.org/wiki/Metaverse>. 08 Nov 2021
- Mishra R, Alam R, Kinahan DJ, Anderson K, Ducrée J (2015) Lipophilic-Membrane Based Routing for Centrifugal Automation of Heterogeneous Immunoassays. In: 2015 28th IEEE International Conference on Micro Electro Mechanical Systems (MEMS 2015). 2015: Estoril, Portugal, pp 523–526 <https://doi.org/10.1109/MEMSYS.2015.7051007>.
- Mishra R, Gaughran J, Kinahan D, Ducrée J (2017) Functional membranes for enhanced rotational flow control on centrifugal microfluidic platforms. In: Reference module in materials science and materials engineering. <https://doi.org/10.1016/b978-0-12-803581-8.04041-8>
- Mishra R, Reilly G, Agnew M, Garvey A, Rogers C, Andrade E, Ma H, Fitzgerald S, Zapatero J, O'Kennedy R, Ducrée J (2018) Laser-actuated centrifugo-pneumatic flow control towards 'sample-to-answer' integrated detection of multi-marker panels at the point-of-care. In: 2018 IEEE Micro Electro Mechanical Systems (MEMS). 2018: Belfast, Northern Ireland, pp 1185–1188 <https://doi.org/10.1109/MEMSYS.2018.8346774>.
- Mishra R, McAuley D, Rolinska N, Boyle D, Ducrée J (2020) Barrier-film based reagent storage and release on microfluidic platforms for sample-to-answer automation of bioassays. In: Lu SLGaH (ed) Proceedings of the 24th International Conference on Miniaturized Systems for Chemistry and Life Sciences (μ TAS 2020), The Chemical and Biological Microsystems Society (CBMS): Virtual, pp 382–383
- Miyazaki CM, Carthy E, Kinahan DJ (2020) Biosensing on the centrifugal microfluidic lab-on-a-disc platform. *Processes* 8:1360. <https://doi.org/10.3390/pr8111360>
- Morais S, Marco-Moles R, Puchades R, Maquieira A (2006) DNA microarraying on compact disc surfaces. Application to the analysis of single nucleotide polymorphisms in Plum pox virus. *Chem Commun (Camb)*. <https://doi.org/10.1039/b600049e>
- Moschou EA, Nicholson AD, Jia GY, Zoval JV, Madou MJ, Bachas LG, Daunert S (2006) Integration of microcolumns and microfluidic fractionators on multitasking centrifugal microfluidic platforms for the analysis of biomolecules. *Anal Bioanal Chem* 385(3):596–605
- Nge PN, Rogers CI, Woolley AT (2013) Advances in microfluidic materials, functions, integration, and applications. *Chem Rev* 113:2550–2583. <https://doi.org/10.1021/cr300337x>
- Nguyen HV, Nguyen VD, Nguyen HQ, Chau THT, Lee EY, Seo TS (2019) Nucleic acid diagnostics on the total integrated lab-on-a-disc for point-of-care testing. *Biosens Bioelectron* 141:111466. <https://doi.org/10.1016/j.bios.2019.111466>
- Olanrewaju A, Beaugrand M, Yafia M, Juncker D (2018) Capillary microfluidics in microchannels: from microfluidic networks to capillary circuits. *Lab Chip* 18:2323–2347. <https://doi.org/10.1039/c8lc00458g>
- Ramachandriaiah H, Amasia M, Cole J, Sheard P, Pickhaver S, Walker C, Wirta V, Lexow P, Lione R, Russom A (2013) Lab-on-DVD: standard DVD drives as a novel laser scanning microscope for image based point of care diagnostics. *Lab Chip* 13(8):1578–1585
- Reyes DR, Iossifidis D, Auroux P-A, Manz A (2002) Micro total analysis systems. 1. Introduction, theory, and technology. *Anal Chem* 74:2623–2636. <https://doi.org/10.1021/ac0202435>
- Reyes DR, Heeren HV, Guha S, Herbertson LH, Tzannis AP, Ducrée J, Bissig H, Becker H (2021) Accelerating innovation and commercialization through standardization of microfluidic-based medical devices. *Lab Chip* 21:9–21. <https://doi.org/10.1039/D0LC00963F>
- Rombach M, Kosse D, Faltin B, Wadle S, Roth G, Zengerle R, von Stetten F (2014) Real-time stability testing of air-dried primers and fluorogenic hydrolysis probes stabilized by trehalose and xanthan. *Biotechniques* 57:151–155. <https://doi.org/10.2144/000114207>
- Rombach M, Hin S, Specht M, Johannsen B, Lüddecke J, Paust N, Zengerle R, Roux L, Sutcliffe T, Peham JR, Herz C, Panning M, Donoso-Mantke O, Mitsakakis K (2020a) RespiDisk: a point-of-care platform for fully automated detection of respiratory tract infection pathogens in clinical samples. *Analyst* 145(21):7040–7047. <https://doi.org/10.1039/d0an01226b>
- Schembri CT, Ostoich V, Lingane PJ, Burd TL, Buhl SN (1992) Portable simultaneous multiple analyte whole-blood analyzer for point-of-care testing. *Clin Chem* 38:1665–1670. <https://doi.org/10.1093/clinchem/38.9.1665>
- Schembri CT, Burd TL, Kopfsill AR, Shea LR, Braynin B (1995) Centrifugation and capillarity integrated into a multiple analyte whole-blood analyzer. *J Autom Chem* 17:99–104. <https://doi.org/10.1155/S1463924695000174>
- Schuler F, Schwemmer F, Trotter M, Wadle S, Zengerle R, von Stetten F, Paust N (2015) Centrifugal step emulsification applied for absolute quantification of nucleic acids by digital droplet RPA. *Lab Chip* 15:2759–2766. <https://doi.org/10.1039/c5lc00291e>
- Schuler F, Trotter M, Geltman M, Schwemmer F, Wadle S, Dominguez-Garrido E, Lopez M, Cervera-Acedo C, Santibanez P, von Stetten F, Zengerle R, Paust N (2016) Digital droplet PCR on disk. *Lab Chip* 16:208–216. <https://doi.org/10.1039/c5lc01068c>
- Schwemmer F, Hutzenlaub T, Buselmeier D, Paust N, von Stetten F, Mark D, Zengerle R, Kosse D (2015a) Centrifugo-pneumatic multi-liquid aliquoting-parallel aliquoting and combination of multiple liquids in centrifugal microfluidics. *Lab Chip* 15:3250–3258. <https://doi.org/10.1039/c5lc00513b>
- Schwemmer F, Zehnle S, Mark D, von Stetten F, Zengerle R, Paust N (2015b) A microfluidic timer for timed valving and pumping in centrifugal microfluidics. *Lab Chip* 15:1545–1553. <https://doi.org/10.1039/C4LC01269K>
- Sciuto EL, Petralia S, Calabrese G, Conoci S (2020) An integrated biosensor platform for extraction and detection of nucleic acids. *Biotechnol Bioeng*. <https://doi.org/10.1002/bit.27290>
- Shea M (2003) ADMET assays on Tecan's LabCD-ADMET system. *J Assoc Lab Autom* 8:74–77. [https://doi.org/10.1016/s1535-5535\(04\)00260-6](https://doi.org/10.1016/s1535-5535(04)00260-6)
- Smith S, Mager D, Perebikovskiy A, Shamloo E, Kinahan D, Mishra R, Delgado SMT, Kido H, Saha S, Ducrée J, Madou M, Land K, Korvink JG (2016a) CD-based microfluidics for primary care in extreme point-of-care settings. *Micromachines*. <https://doi.org/10.3390/mi7020022>

- Smith S, Sewart R, Becker H, Roux P, Land K (2016b) Blister pouches for effective reagent storage on microfluidic chips for blood cell counting. *Microfluid Nanofluid*. <https://doi.org/10.1007/s10404-016-1830-2>
- SpinX Technologies. Available on: <https://web.archive.org/web/20040414090409/http://www.spinx-technologies.com/>. 15 Jun 2021
- Stavis SM (2012) A glowing future for lab on a chip testing standards. *Lab Chip* 12:3008–3011. <https://doi.org/10.1039/c2lc40511c>
- Steigert J, Brenner T, Grumann M, Riegger L, Lutz S, Zengerle R, Ducrée J (2007) Integrated siphon-based metering and sedimentation of whole blood on a hydrophilic lab-on-a-disk. *Biomed Microdev* 9:675–679. <https://doi.org/10.1007/s10544-007-9076-0>
- Strohmeier O, Keil S, Kanat B, Patel P, Niedrig M, Weidmann M, Hufert F, Drexler J, Zengerle R, von Stetten F (2015a) Automated nucleic acid extraction from whole blood, *B. subtilis*, *E. coli*, and Rift Valley fever virus on a centrifugal microfluidic LabDisk. *RSC Adv* 5:32144–32150. <https://doi.org/10.1039/c5ra03399c>
- Strohmeier O, Keller M, Schwemmer F, Zehnle S, Mark D, von Stetten F, Zengerle R, Paust N (2015b) Centrifugal microfluidic platforms: advanced unit operations and applications. *Chem Soc Rev* 44:6187–6229. <https://doi.org/10.1039/c4cs00371c>
- Tang M, Wang G, Kong S-K, Ho H-P (2016) A review of biomedical centrifugal microfluidic platforms. *Micromachines*. <https://doi.org/10.3390/mi7020026>
- Thompson BL, Birch C, Nelson DA, Li J, DuVall JA, Le Roux D, Tsuei AC, Mills DL, Root BE, Landers JP (2016a) A centrifugal microfluidic device with integrated gold leaf electrodes for the electrophoretic separation of DNA. *Lab Chip* 16:4569–4580. <https://doi.org/10.1039/c6lc00953k>
- Thompson BL, Gilbert RJ, Mejia M, Shukla N, Haverstick DM, Garner GT, Landers JP (2016b) Hematocrit analysis through the use of an inexpensive centrifugal polyester-toner device with finger-to-chip blood loading capability. *Anal Chim Acta* 924:1–8. <https://doi.org/10.1016/j.aca.2016.04.028>
- Tijero M, Díez-Ahedo R, Benito-Lopez F, Basabe-Desmonts L, Castro-López V, Valero A (2015) Biomolecule storage on non-modified thermoplastic microfluidic chip by ink-jet printing of ionogels. *Biomicrofluidics* 9:044124. <https://doi.org/10.1063/1.4928300>
- Torres-Delgado SM, Kinahan DJ, Nirupa-Julius LA, Mallette A, Ardila DS, Mishra R, Miyazaki CM, Korvink JG, Ducrée J, Mager D (2018) Wirelessly powered and remotely controlled valve-array for highly multiplexed analytical assay automation on a centrifugal microfluidic platform. *Biosens Bioelectron* 109:214–223. <https://doi.org/10.1016/j.bios.2018.03.012>
- van Heeren H (2012) Standards for connecting microfluidic devices? *Lab Chip* 12:1022–1025. <https://doi.org/10.1039/C2LC20937C>
- Wang Y, Li Z, Huang X, Ji W, Ning X, Liu K, Tan J, Yang J, Ho H-P, Wang G (2019) On-board control of wax valve on active centrifugal microfluidic chip and its application for plasmid DNA extraction. *Microfluid Nanofluid*. <https://doi.org/10.1007/s10404-019-2278-y>
- Watts AS, Urbas AA, Moschou E, Gavalas VG, Zoval JV, Madou M, Bachas LG (2007) Centrifugal microfluidics with integrated sensing microdome optodes for multiion detection. *Anal Chem* 79:8046–8054. <https://doi.org/10.1021/ac0709100>
- Whitesides GM (2006) The origins and the future of microfluidics. *Nature* 442:368–373. <https://doi.org/10.1038/nature05058>
- Yao Y, Kshirsagar M, Vaidya G, Ducrée J, Ryan C (2021) Convergence of blockchain, autonomous agents, and knowledge graph to share electronic health records. *Front Blockchain*. <https://doi.org/10.3389/fbloc.2021.661238>
- Yuan X, Oleschuk RD (2018) Advances in microchip liquid chromatography. *Anal Chem* 90:283–301. <https://doi.org/10.1021/acs.analchem.7b04329>
- Zehnle S, Schwemmer F, Bergmann R, von Stetten F, Zengerle R, Paust N (2015) Pneumatic siphon valving and switching in centrifugal microfluidics controlled by rotational frequency or rotational acceleration. *Microfluid Nanofluid* 19:1259–1269. <https://doi.org/10.1007/s10404-015-1634-9>
- Zehnle S, Rombach M, Zengerle R, von Stetten F, Paust N (2017) Network simulation-based optimization of centrifugopneumatic blood plasma separation. *Biomicrofluidics*. <https://doi.org/10.1063/1.4979044>
- Zhang X, Wasserberg D, Breukers C, Terstappen LWMM, Beck M (2016) Controlled antibody release from gelatin for on-chip sample preparation. *Analyst* 141:3068–3076. <https://doi.org/10.1039/c5an02090e>
- Zhao Y, Schwemmer F, Zehnle S, von Stetten F, Zengerle R, Paust N (2015) Centrifugo-pneumatic sedimentation, re-suspension and transport of microparticles. *Lab Chip* 15:4133–4137. <https://doi.org/10.1039/c5lc00508f>

Publisher's Note Springer Nature remains neutral with regard to jurisdictional claims in published maps and institutional affiliations.